https://doi.org/10.1093/plcell/koad176 THE PLANT CELL 2023: 35: 3845–3869

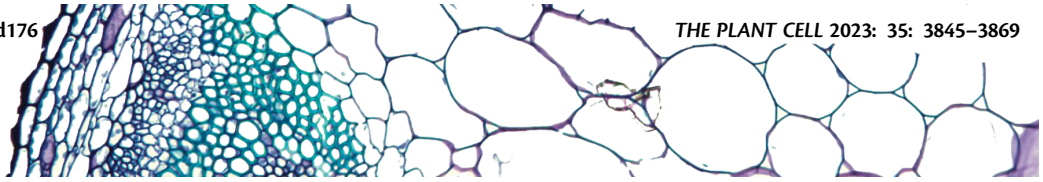

Research Article

dsRNA-induced immunity targets plasmodesmata and is suppressed by viral movement proteins

Caiping Huang [1,†] Ana Rocío Sede [1,†] Laura Elvira-González [1,†] Yan Yan [2] Miguel Eduardo Rodriguez [2] Jérôme Mutterer [1] Emmanuel Boutant [1,‡] Libo Shan [2] and Manfred Heinlein [1,*]

1 Institut de biologie moléculaire des plantes, CNRS, Université de Strasbourg, 67000 Strasbourg, France
2 Department of Biochemistry and Biophysics, College of Agriculture and Life Sciences, Texas A&M University, College Station, TX 77843, USA

*Author for correspondence: heinlein@unistra.fr
†Equal contribution.
‡Present address: UMR 7021, CNRS, Laboratoire de Bioimagerie et Pathologies, Université de Strasbourg, Faculté de Pharmacie, 67400 Illkirch, France.
The author responsible for distribution of materials integral to the findings presented in this article in accordance with the policy described in the Instructions for Authors (https://academic.oup.com/plcell/pages/General-Instructions) is: Manfred Heinlein (heinlein@unistra.fr).

Abstract

Emerging evidence indicates that in addition to its well-recognized functions in antiviral RNA silencing, dsRNA elicits pattern-triggered immunity (PTI), likely contributing to plant resistance against virus infections. However, compared to bacterial and fungal elicitor-mediated PTI, the mode-of-action and signaling pathway of dsRNA-induced defense remain poorly characterized. Here, using multicolor in vivo imaging, analysis of GFP mobility, callose staining, and plasmodesmal marker lines in *Arabidopsis thaliana* and *Nicotiana benthamiana*, we show that dsRNA-induced PTI restricts the progression of virus infection by triggering callose deposition at plasmodesmata, thereby likely limiting the macromolecular transport through these cell-to-cell communication channels. The plasma membrane-resident SOMATIC EMBRYOGENESIS RECEPTOR-LIKE KINASE 1, the BOTRYTIS INDUCED KINASE1/AVRPPHB SUSCEPTIBLE1-LIKE KINASE1 kinase module, PLASMODESMATA-LOCATED PROTEINs 1/2/3, as well as CALMODULIN-LIKE 41 and Ca^{2+} signals are involved in the dsRNA-induced signaling leading to callose deposition at plasmodesmata and antiviral defense. Unlike the classical bacterial elicitor flagellin, dsRNA does not trigger a detectable reactive oxygen species (ROS) burst, substantiating the idea that different microbial patterns trigger partially shared immune signaling frameworks with distinct features. Likely as a counter strategy, viral movement proteins from different viruses suppress the dsRNA-induced host response leading to callose deposition to achieve infection. Thus, our data support a model in which plant immune signaling constrains virus movement by inducing callose deposition at plasmodesmata and reveals how viruses counteract this layer of immunity.

Introduction

The virome of plants is dominated by RNA viruses (Dolja et al. 2020), and several of these cause devastating diseases in cultivated plants leading to global crop losses (Jones and Naidu 2019; Jones 2021). To infect plants, RNA viruses engage in complex interactions with compatible plant hosts. In cells at the spreading infection front, RNA viruses associate with cellular membranes and replicate their genome through dsRNA intermediates. Moreover, they use their movement proteins (MPs) to interact with membrane-associated transport processes in order to achieve the movement of replicated genome copies through cell wall nanochannels called plasmodesmata (PD) and, thereby, to infect new cells (Heinlein 2015). Importantly, sensing of viral dsRNA by the host triggers defense responses against infection; viruses must be able to control these responses to propagate.

Received November 21, 2022. Accepted May 23, 2023. Advance access publication June 28, 2023

IN A NUTSHELL

Background: Plants employ different defense mechanisms against pathogens. The major mechanism that plants use for defense against viruses is known as RNA silencing. This mechanism is triggered by the presence of viral double-stranded (ds)RNA and uses small RNAs to inhibit viral replication by targeting the viral genome for degradation. Recently, it was found that dsRNA elicits antiviral defense also through a protein-mediated response known as pattern-triggered immunity (PTI). However, the underlying mechanism of antiviral PTI and how viruses overcome this plant defense mechanism to cause infection is unknown.

Question: In this study, we asked how dsRNA-induced PTI acts to inhibit virus infection and whether we can identify components of the PTI signaling pathway. Moreover, we wanted to know how viruses overcome this plant host defense response in order to cause infection.

Findings: We demonstrate that dsRNA-induced PTI targets plasmodesmata (PD), the intercellular communication conduits in plant cell walls that viruses use to spread infection from cell to cell. By inducing the deposition of callose, dsRNA-induced PTI reduces PD permeability, thus restricting virus movement. We identified PTI signaling components required for dsRNA-induced PD callose deposition and delineate a PTI pathway showing important differences to PTI pathways triggered by microbial elicitors. Moreover, viral movement proteins (MPs) suppress the dsRNA-induced callose deposition response at PD. This leads to a model of how plant immune signaling constrains virus movement and how viruses counteract this layer of immunity.

Next steps: This study calls upon the identification of the PTI dsRNA receptor and the mechanisms of PTI signaling (involving identified components such as SOMATIC EMBRYOGENESIS RECEPTOR-LIKE KINASE 1, BOTRYTIS INDUCED KINASE1, calcium channels, CALMODULIN-LIKE protein 41, PDLP1/2/3) and PTI suppression by MPs, and how dsRNA-induced PTI and RNA silencing are controlled during the spread of infection.

The most important antiviral host response in plants is RNA silencing (Lopez-Gomollon and Baulcombe 2022). It involves host DICER-LIKE enzymes that inhibit viral replication by cleaving the viral dsRNA replication intermediate into small interfering RNAs (siRNAs). These viral siRNAs can associate with ARGONAUTE proteins in RNA-induced silencing complexes to further guide the sequence-specific degradation and translational suppression of viral RNA. To control this antiviral response and to enhance their replication, viruses have evolved specific effector proteins (viral suppressor of RNA silencing, VSR) that interfere with the RNA silencing pathway at distinct steps (Csorba et al. 2015).

More recent research has shown that in addition to the antiviral RNA silencing response, RNA virus infection also activates pattern-triggered immunity (PTI) (Kørner et al. 2013), whereby dsRNA acts as an important elicitor (Niehl et al. 2016). Unlike RNA silencing, PTI is triggered by specific recognition of conserved microbe-associated molecular pattern or pathogen-associated molecular pattern (PAMP) by pattern-recognition receptors (PRRs) and the induction of defense signaling (DeFalco and Zipfel 2021). Importantly, dsRNA-induced PTI is independent of dsRNA sequence. Thus, PTI is activated by viral dsRNA and by nonviral dsRNA, for example GFP dsRNA.

PTI can also be activated by the synthetic dsRNA analog polyinosinic-polycytidilic acid [poly(I:C)] (Niehl et al. 2016), a well-known ligand of the dsRNA-perceiving TLR3-receptor in animals (Alexopoulou et al. 2001). Similar to virus replication, treatment of *Arabidopsis thaliana* plants with poly(I:C) elicits antiviral defense along with activating typical PTI responses, such as mitogen-activated protein kinase (MPK) activity, ethylene production, seedling root growth inhibition, and marker gene expression (Kørner et al. 2013; Niehl et al. 2016). Poly(I:C)-triggered ethylene production and antiviral defense were shown to depend on the coreceptor kinase SOMATIC EMBRYOGENESIS RECEPTOR-LIKE KINASE 1 (SERK1) (Niehl et al. 2016) but neither other components of the signaling pathway nor the mechanism by which PTI restricts virus infection are known.

Here, we demonstrate that unlike RNA silencing, which controls viral RNA accumulation, dsRNA-induced PTI acts on PD to restrict virus movement. Additional components of the PTI signaling mechanism to PD are identified and shown to be critical for limiting virus infection and symptom formation. Moreover, the observations indicate that the cell-to-cell propagation of virus infection is linked to the ability of the viral MP to suppress the dsRNA-induced defense response leading to PD closure. Taken together, the results draw a central role of PTI signaling and suppression in determining the ability of viruses to spread infection between cells in susceptible plants.

Results

dsRNA causes inhibition of virus movement in *Nicotiana benthamiana*

To discover how dsRNA-induced PTI inhibits RNA virus infection, we visualized the effect of poly(I:C) treatment on local infections of *N. benthamiana* plants using tobacco mosaic virus tagged with GFP (TMV-GFP). The TMV-GFP infection sites were lower in number and smaller in plants treated with poly(I:C) or with a bacterial PTI elicitor derived from

flagellin (flg22) than in control plants treated with water (Fig. 1, A and B; Supplemental Fig. S1). The treatments did not cause a significant change in GFP fluorescence intensity, an indicative for viral replication and accumulation (Fig. 1A) indicating that they may not exert a significant bulk effect on viral RNA accumulation in infected cells.

To test this further, we measured the accumulation of viral RNA in leaves agroinfiltrated for expression of a cell-autonomous, MP-deficient TMV replicon (TMVΔMPΔCP-GFP). As shown in Fig. 1C, pretreatment of the leaves with poly(I:C) did not elicit a significant effect on TMVΔMΔC-GFP viral accumulation through a time-course of infection at 1, 3, and 5 d post infection (dpi) compared to leaves treated with water. Therefore, the reduced size and number of infection sites in poly(I:C)-treated leaves suggested that the poly(I:C)-triggered immunity may be linked to the reduced cell-to-cell movement of the virus.

dsRNA triggers callose deposition at PD along with the activation of typical PTI responses in *N. benthamiana*

Because virus intercellular movement occurs through PD (Heinlein 2015), we hypothesized that dsRNA inhibits virus movement by causing PD closure. A major mechanism restricting the conductivity of PD for the transport of macromolecules involves the deposition of callose (β-1,3-glucan) in the cell wall region surrounding the PD channel (Wu et al. 2018). Consistently, treatment of *N. benthamiana* plants with poly(I:C), flg22, or water, and quantification of PD-associated callose by in vivo aniline blue staining (Huang et al. 2022) revealed that both poly(I:C) and flg22 trigger increased levels of PD-associated callose in a concentration-dependent manner (Fig. 1, D and E).

Induction of callose at PD is also seen upon treatment of *N. benthamiana* plants with Phi6 dsRNA (Niehl et al. 2018) (Fig. 1F), which dismisses the possibility that poly(I:C) induced callose deposition through an unspecific effect. In agreement with poly(I:C)-induced callose deposition at PD, poly(I:C)-treated tissues showed reduced PD permeability as determined by a GFP mobility assay. In this assay, isolated individual cells of *N. benthamiana* leaves were transformed for the expression of cytoplasmic GFP together with red fluorescent protein tagged with a nuclear localization signal (NLS-RFP) as a red fluorescent cell-autonomous marker (Fig. 1G). Whereas more than 97% of the observed GFP-expressing cells showed GFP mobility into one or 2 adjacent cell layers in control (water)-treated tissues, this mobility was reduced to 31% in the presence of poly(I:C) (Fig. 1H). The differences in data distributions and the reduction of GFP movement mean values from 1.3 cell layers in control-treated tissues to 0.3 cell layers in poly(I:C) treated tissues were statistically significant, as shown by Mann–Whitney and bootstrapping tests (Johnston and Faulkner 2021), respectively (Fig. 1I). As previously noted in Arabidopsis (Niehl et al. 2016), poly(I:C) triggered a moderate MPK activation and the level of activation was significantly weaker than the activation observed with flg22 (Fig. 1J). Moreover, poly(I:C)-treated leaves exhibited the induction of *N. benthamiana* defense-related genes, such as genes encoding BOTRYTIS INDUCED KINASE1 (BIK1), PATHOGENESIS-RELATED PROTEIN 2 (PR2), NADPH/RESPIRATORY BURST OXIDASE PROTEIN B (RBOHB), and ENHANCED DISEASE SUSCEPTIBILITY 1 (EDS1), whereas the gene for BRASSINOSTEROID INSENSITIVE 1 (BRI1) was downregulated (Fig. 1K).

Poly(I:C)-induced PD callose deposition in Arabidopsis requires PTI signaling components but is independent of ROS and MPK

To determine how dsRNA elicits the deposition of callose at PD, we turned our attention to Arabidopsis. As noted previously (Niehl et al. 2016), the treatment of *A. thaliana* Col-0 plants with poly(I:C) causes a significant induction in some PTI-related gene expression, including *SERK1* (Fig. 2A). Among the tested genes, only the induction of *PR5* was found to be SERK1-dependent (Fig. 2B), thus suggesting the participation of SERK1-independent mechanisms in dsRNA sensing. Importantly, treatment with poly(I:C) as well as treatment with 50 ng/μL Phi6 dsRNA increased the PD-associated callose levels as seen before in *N. benthamiana* (Fig. 2, C and D). The induced callose depositions are exactly localized to PD as shown in transgenic *A. thaliana* Col-0 plants expressing PD markers PLASMODESMATA CALLOSE BINDING 1 fused to the red fluorescent protein mCHERRY (mCherry-PDCB1) or PLASMODESMATA-LOCALIZED β-1,3-GLUCANASE 2 fused to the yellow fluorescent protein mCitrine (PdBG2-mCitrine) (Benitez-Alfonso et al. 2013) (Fig. 2, E and F).

Interestingly, dsRNA-induced callose deposition was strongly inhibited in *bik1 pbl1* plants (Fig. 2G), which are deficient in the receptor-like cytoplasmic kinase (RLCK) BIK1 and its homolog PBS1-LIKE KINASE1 (PBL1). The BIK1 RLCK module is an important component of PTI signaling that integrates signals from multiple PRRs, as shown by its direct interaction with the PRR proteins FLAGELLIN SENSITIVE 2 (FLS2), EF-TU RECEPTOR, PEPTIDE RECEPTOR (PEPR)1 and PEPR2, and CHITIN ELICITOR RECEPTOR KINASE 1 (Lu et al. 2010; Zhang et al. 2010; Liu et al. 2013), and its ability to phosphorylate and activate downstream targets, such as the NADPH Oxidase RESPIRATORY BURST OXIDASE HOMOLOG D (Kadota et al. 2014). BIK1 and PBL1 have additive effects; unlike the single mutants, the *bik1 pbl1* double mutant was shown to strongly inhibit PAMP-induced defense responses (Zhang et al. 2010). In addition, *bik1 pbl1* plants are also deficient in poly(I:C)-induced MPK activation and seedling root growth inhibition as compared to Col-0 wild-type (WT) plants (Fig. 2, H and I).

Perception of flg22 by the FLS2 and BRI1-ASSOCIATED RECEPTOR KINASE1 (BAK1) coreceptor complex induces rapid phosphorylation of BIK1, evidenced by a protein mobility shift in immunoblotting analysis (Lu et al. 2010; Zhang et al. 2010). To determine if BIK1 is phosphorylated in the presence of poly(I:C), Arabidopsis WT Col-0 protoplasts expressing HA epitope-tagged BIK1 were treated with poly(I:C)

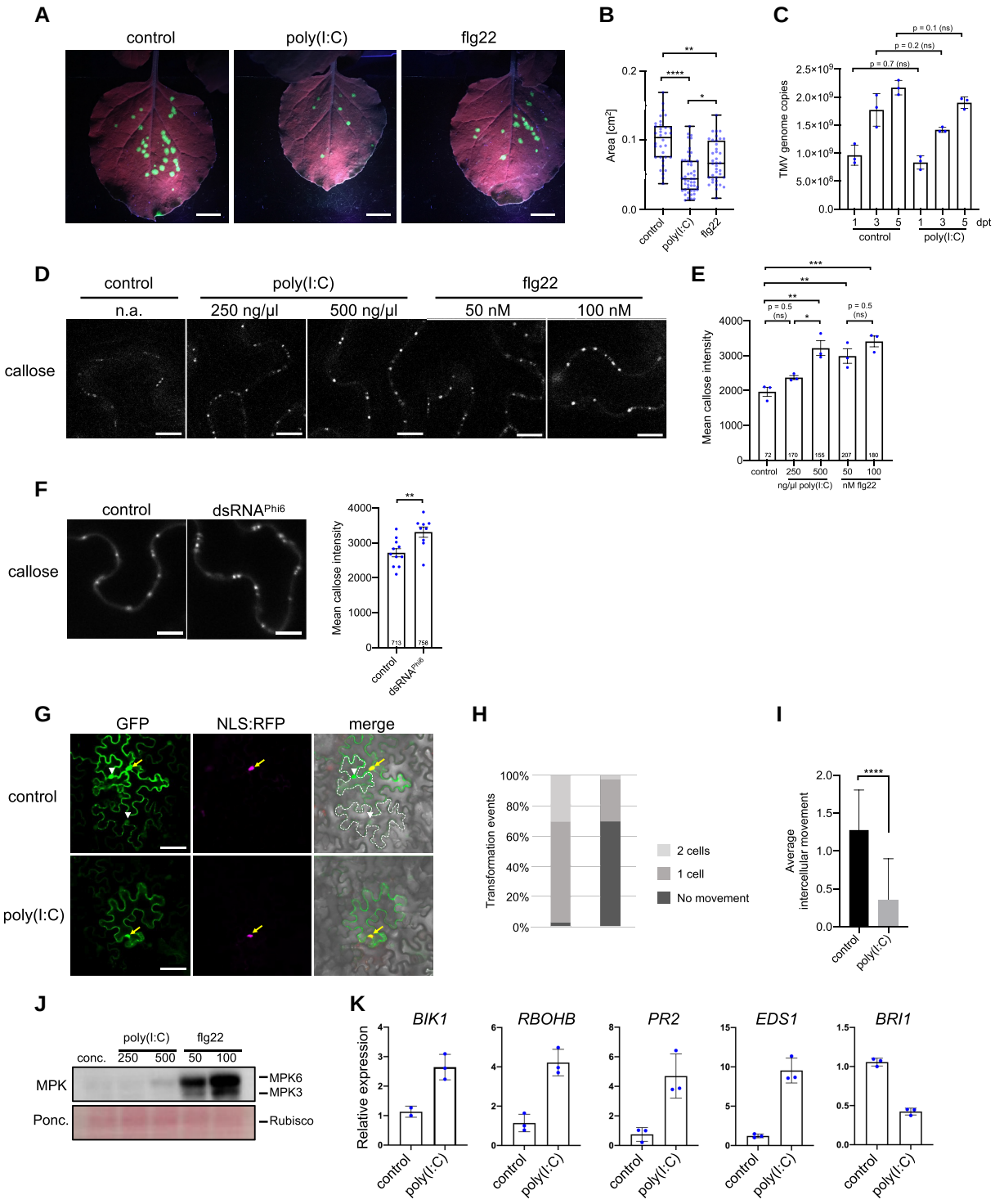

Figure 1. Poly(I:C) treatment causes inhibition of virus movement in *N. benthamiana*. **A)** TMV-GFP infection sites in *N. benthamiana* leaves at 7 dpi treated with the virus together with either water (control), 0.5 $\mu g/\mu L$ (≈1 μM) poly(I:C), or 1 μM flg22. Scale bar, 1 cm. **B)** Sizes of individual infection sites measured in 10 leaf samples collected from 3 plants per treatment. Kruskal–Wallis test ($P = <0.0001$) followed by Dunn's test for pairwise comparisons; ****, $P = <0.0001$; **, $P = <0.01$; *, $P = <0.05$. The experiment was performed 3 times with similar results. **C)** TMV replication in *N. benthamiana* is not influenced by poly(I:C). A cell-autonomous, MP-deficient TMV replicon (TMVΔMPΔCP-GFP) expressed in cells of agroinoculated leaves produces the same number of RNA genome copies in the presence and absence of treatment with 0.5 $\mu g/\mu L$ poly(I:C), as determined by Taqman RT-qPCR. Poly(I:C) and control treatments were applied 1 d after agroinoculation and results obtained at indicated days after this treatment (dpt) are shown. The data represent means of 3 biological replicates (with standard deviation) per time point and treatment. Two-tailed Mann–Whitney test. **D and E)** Treatment of *N. benthamiana* with poly(I:C) or flg22 induces increased callose deposition at PD within 30 min in a dose-specific manner. **D)** Callose fluorescence at PD upon aniline blue staining. Scale bar, 10 μm. **E)** Mean callose content in PD determined

(continued)

for 20 min. Subsequent immunoblot analysis with anti HA-antibody revealed that similar to flg22 treatment, poly(I:C) treatment induces a mobility shift of BIK1-HA proteins (Fig. 3A). BIK1 phosphorylation was confirmed by the absence of this mobility shift in the presence of calf intestine phosphatase (CIP) (Fig. 3, A and B) or the protein kinase inhibitor K-252a (Fig. 3B). Taken together, the data suggest the involvement of BIK1/PBL1 in dsRNA-triggered immunity mediating the callose deposition at the PD.

Previously, we observed that *serk1-1* mutants show reduced levels of poly(I:C)-induced ethylene production and antiviral protection (Niehl et al. 2016). We further investigated the involvement of SERK1 in poly(I:C)-induced BIK1 phosphorylation. As shown in Fig. 3C, the level of poly(I:C)-induced BIK1 phosphorylation was increased upon SERK1 overexpression in WT Col-0 plants and decreased in the *serk1-1* mutant. Importantly, the poly(I:C)-induced PD callose deposition was drastically reduced in *serk1-1* mutants compared to WT Col-0 plants (Fig. 3, D and E). Whereas the mean PD callose level increased by 40% in WT Col-0 plants upon poly(I:C) treatment, only a minor increase (5%) in the PD callose level was observed in the *serk1* mutant. Thus, the data indicate that SERK1 contributes to poly(I:C)-induced BIK1 phosphorylation and may function genetically upstream of BIK1. The remaining small but statistically significant, poly(I:C)-induced increase in PD callose deposition observed in the *serk1* mutant is consistent with the involvement of additional coreceptors in dsRNA-sensing.

To investigate the poly(I:C)-induced signaling pathway downstream of BIK1, we examined the production of reactive oxygen species (ROS) by a luminescence assay. ROS play important roles in plant development and stress responses (Mittler 2017) and are also produced during infections with fungal and bacterial pathogens (Castro et al. 2021). ROS accumulate also upon perception of the fungal and bacterial elicitors chitin and flagellin (flg22) (Nühse et al. 2007; Cheval et al. 2020) and have been linked to local and systemic signaling, including calcium signaling, and the deposition of callose at PD (Faulkner et al. 2013; Cheval et al. 2020). Notably, neither the treatment of Arabidopsis Col-0 plants (Fig. 4A) nor the treatment of *N. benthamiana* plants (Fig. 4B) with poly(I:C) led to the production of ROS. By contrast, strong responses were recorded in both plant species upon treatment with the flg22 elicitor. Thus, unlike for chitin and flagellin (flg22), the signaling induced by poly(I:C) does not involve ROS species detectable by luminescent assays (notably hydrogen peroxide).

Moreover, *mpk3* and *mpk6* single mutants that are deficient for the mitogen-activated protein kinases (MPK) 3 and 6, respectively, as well as the *mpk3 amiRmpk6* mutants (a *mpk3* mutant in which *MPK6* is silenced by an artificial miRNA) (Li et al. 2014) showed increased levels of callose at PD upon poly(I:C) treatment similar to WT plants (Fig. 4C). Considering the relatively weak activation of MPKs by poly(I:C) treatment (Figs. 1J and 2H), it is possible that the MPK3/6 module may not play a major role in dsRNA-induced callose deposition. Alternatively, it is also possible that additional yet non-identified MPKs may be involved in this process.

To further investigate the signaling pathway induced by dsRNA, additional mutants were tested. We started with Arabidopsis mutants deficient in the PD-localized proteins (PDLPs), which are a family of eight proteins that dynamically regulate PD (Thomas et al. 2008). PDLP5 plays a nonredundant role in intercellular systemic acquired resistance signaling (Lim et al. 2016) and in mediating salicylic acid (SA)-induced PD closure, a process required for resistance against the bacterial pathogen *Pseudomonas syringae* (Lee et al. 2011; Wang et al. 2013). However, *pdlp5* mutant plants showed strong callose deposition at PD upon poly(I:C) treatment (Fig. 4D), indicating that dsRNA-induced callose deposition is independent of PDLP5 and of a potential SA response mediated by this protein. Next, we tested PDLP1, PDLP2 and PDLP3, which play redundant roles in callose deposition at PD (Thomas et al. 2008), in callose deposition within haustoria formed in response to infection by mildew fungus (Caillaud et al. 2014), and also as binding

(**Figure 1.** Continued)
in 3 leaf disks per treatment (dots). The total number of evaluated PD is given at the base of each column. Error bars show the SEM. Parametric mean value variances between conditions were statistically tested by ANOVA ($P = 0.0004$) followed by Sidak's pairwise comparisons. ***, $P = <0.001$; **, $P = < 0.01$; ns = nonsignificant. **F)** Callose deposition at PD in *N. benthamiana* leaf epidermal tissue upon treatment with 50 ng/μL biological dsRNA ($dsRNA^{Phi6}$). Mean callose content in PD determined in 9 leaf disks from 3 plants per treatment (dots). Two-tailed *t*-test; **, $P = <0.01$. **G to I)** GFP mobility assay in *N. benthamiana*. Leaf disks expressing GFP together with cell-autonomous NLS:RFP 1 d after agroinfiltration were treated with water or 0.5 μg/μL poly(I:C) and imaged 48 h later. **G)** Example of GFP movement from an epidermal cell marked by cell-autonomous NLS:RFP into adjacent cells. Transiently expressed GFP shows a nucleocytoplasmic distribution (yellow arrow) and its movement from the expressing epidermal cell (coexpressed NLS:RFP in the nucleus, in magenta) is evident by appearance of green fluorescence in the nuclei and cytoplasm of adjacent cells (white arrowheads). Cells into which GFP moved are indicated by the white dashed line in the merged image. Scale bar, 50 μm. **H and I)** Quantification of GFP movement between epidermal cells in leaf disks exposed to 0.5 μg/μL poly(I:C) or water (control) (29 transformation events were analyzed for each treatment). **H)** Stacked column diagram showing the relative frequency of transformation events associated with either no GFP movement (dark gray), GFP movement into one adjacent cell layer (medium gray), or GFP movement into 2 adjacent cell layers (light gray). **I)** Average intercellular movement (total number of cell layers into which GFP has moved divided by the number of evaluated transformation events). Two-tailed Mann–Whitney test; ****, $P = <0.0001$. Bootstrap test; #, $P = <0.05$. A repetition of the GFP mobility assay provided similar results. **J)** Low level of MPK activation by poly(I:C) relative to flg22 after 30 min. Concentrations (conc.) are in ng/μL for poly(I:C) and nM for flg22. The experiment was performed 3 times with similar results. **K)** Poly(I:C) induces innate immunity marker genes but suppresses expression of *BRI1* in *N. benthamiana*. Mean values and standard deviations of gene expression values obtained by RT-qPCR with 3 biological replicates (dots) harvested 3 h after treatment. ns, not significant.

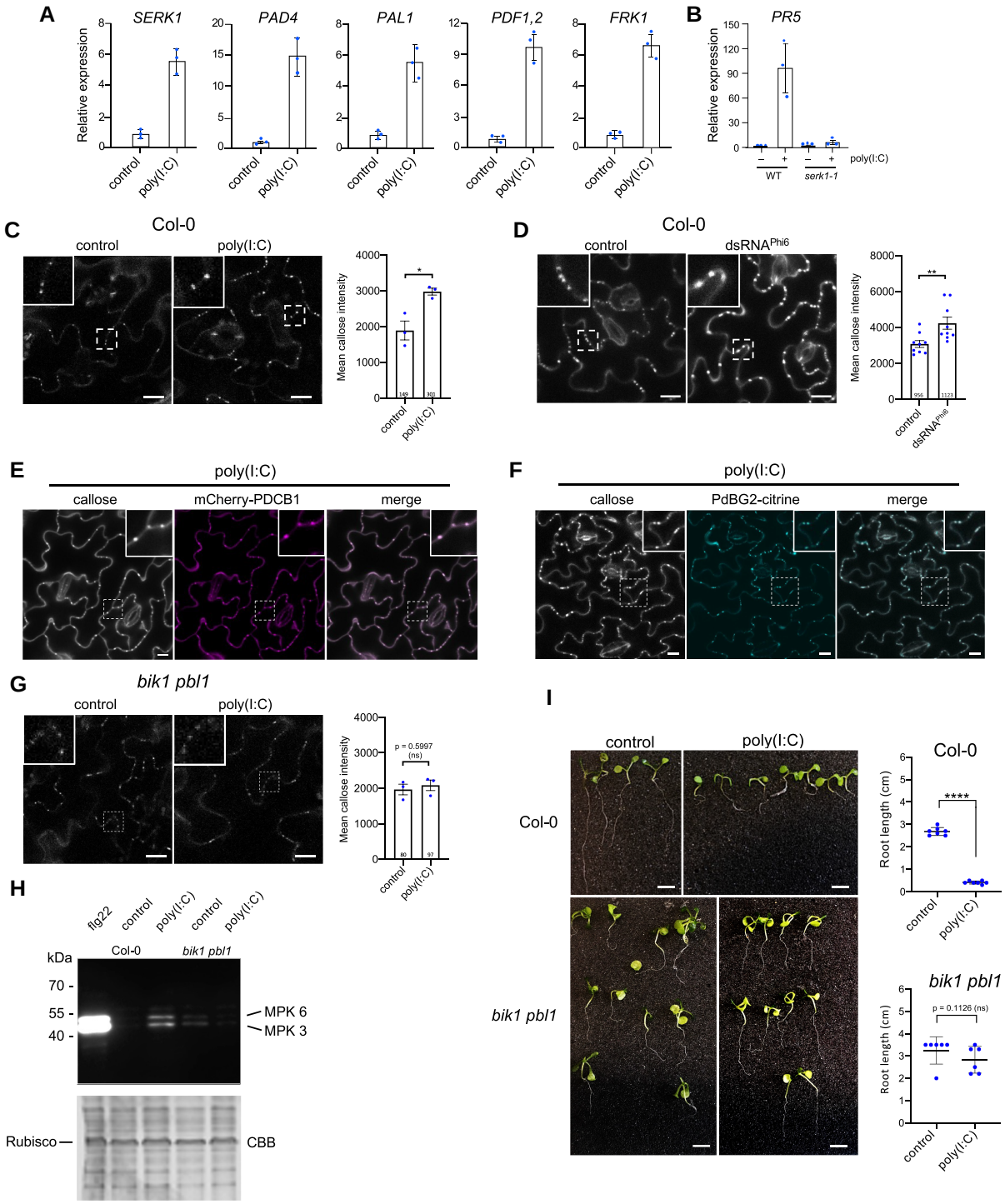

Figure 2. Poly(I:C)-induced signaling in Arabidopsis depends on BIK1/PBL1. **A** and **B)** Transcriptional regulation of Arabidopsis genes 3 h after treatment with 0.5 μg/μL poly(I:C). For each gene, the mean value and the standard deviation of gene expression values obtained by RT-qPCR analysis of 3 biological replicates (dots) is shown. **A)** Poly(I:C) induces innate immunity marker genes in *A. thaliana* Col-0 wildtype. **B)** Absence of poly(I:C)-induced *PR5* expression in the *serk1-1* mutant. **C)** Poly(I:C) treatment causes callose deposition at PD in *A. thaliana* Col-0. Images were taken 30 min after treatment. Inlays show enlargements of the areas within the dashed boxes. Scale bar, 20 μm. Mean callose content in PD determined in 3 leaf disks from 3 plants per treatment (dots). The total number of evaluated PD is given at the base of each column. Error bars show the SEM. Two-tailed *t*-test; *, $P = <0.05$. **D)** Callose deposition at PD in *A. thaliana* Col-0 leaf epidermal tissue 30 min after treatment with 50 ng/μL of biological dsRNA (dsRNA^{Phi6}). Inlays show enlargements of the areas within the dashed boxes. Scale bar, 20 μm. Mean callose content in PD determined in 9 leaf disks from 3 plants per treatment (dots). The total number of evaluated PD is given at the base of each column. Error bars show the SEM. Two-tailed *t*-test; **, $P = <0.01$. **E** and **F)** Poly(I:C)-induced callose spots are localized to PD as shown by colocalization with PD markers mCherry-PDCB1 **E**) and PdBG2-citrine **F**). Inlays show enlargements of the areas within the dashed boxes. Scale bar, 10 μm. **G)** poly(I:C)-induced

(continued)

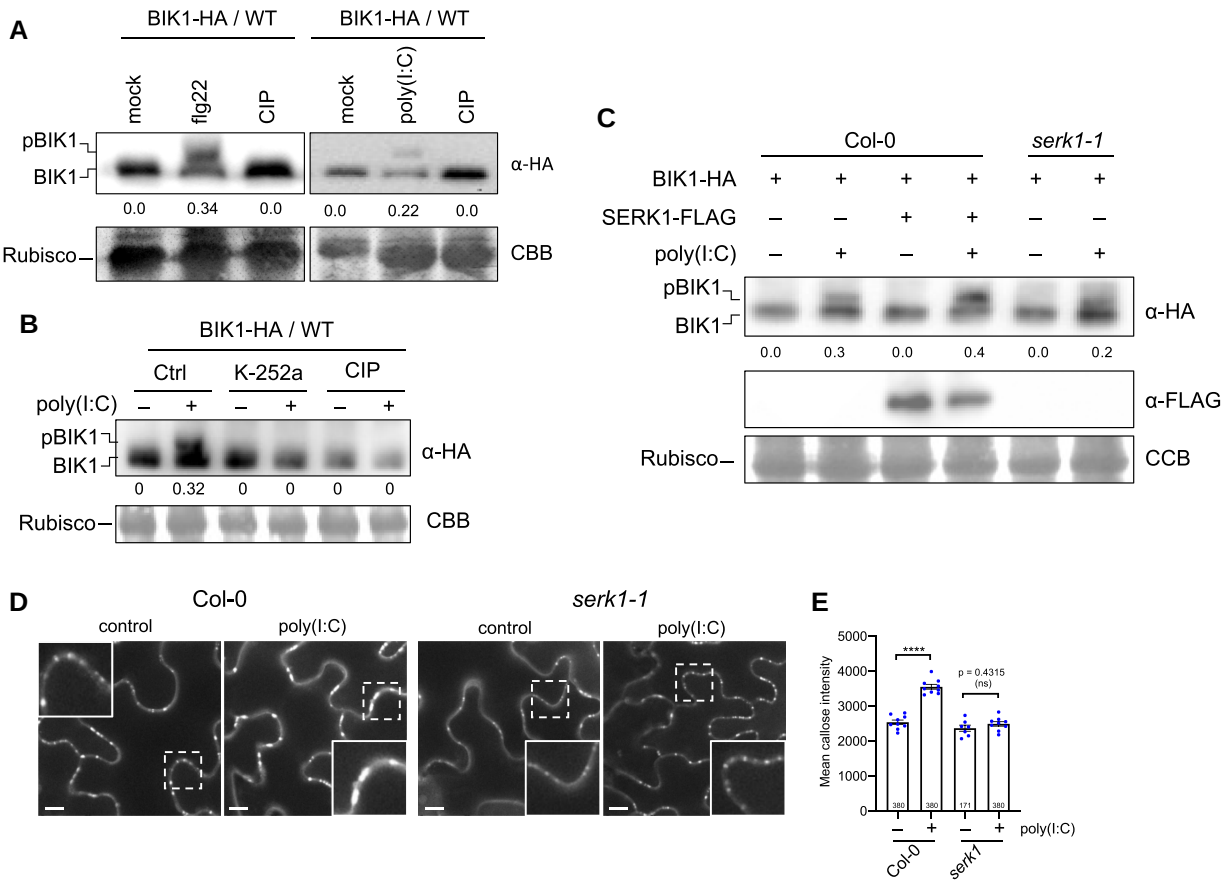

Figure 3. Poly(I:C) causes BIK1 phosphorylation and PD callose deposition in a SERK1-dependent manner. **A** to **C**) Analysis of BIK1 phosphorylation in poly(I:C)-treated *A. thaliana* Col-0 protoplasts. **A)** Poly(I:C) treatment induces BIK1 phosphorylation as shown by a protein mobility shift detected by immunoblot analysis. Protoplasts expressing BIK1-HA were nontreated (mock) or treated with 1 μM flg22 or 0.5 μg/μL poly(I:C), lysed after 20 min and treated or nontreated with CIP for 1 h before immunoblot analysis using HA-HRP antibody. BIK1 band intensities were quantified using Image Lab (Bio-Rad). Quantification of BIK1 phosphorylation (upper panel) calculated as ratio of intensity of the upper band (phosphorylated BIK1, pBIK1) to the sum intensities of shifted and nonshifted bands (pBIK1 + BIK1) (no treatment set to 0.0). CCB, Coomassie Brilliant Blue staining of Rubisco as gel loading control (lower panel). **B)** Poly(I:C)-induced BIK1 phosphorylation is blocked by 1 μM of the kinase inhibitor K-252a added 1 h before poly(I:C) treatment. Rubisco detection by CBB staining is shown as gel loading control (lower panel). Experimental conditions and quantification of BIK1 phosphorylation as in **A**). **C)** SERK1 enhances poly(I:C)-induced BIK1 phosphorylation. Protoplasts from WT Col-0 or *serk1-1* mutants were transfected with BIK1-HA together with or without SERK1-FLAG and followed by treatment with or without 0.5 μg/μL poly(I:C). Phosphorylated BIK1 band intensities were quantified as in **A**). The middle panel shows SERK1-FLAG expression. Rubisco detection by CBB staining is shown as gel loading control (lower panel). **D and E)** Efficient poly(I:C)-induced PD callose deposition depends on SERK1. **D)** Callose fluorescence at PD seen upon aniline blue staining of epidermal cells of WT Col-0 plants and *serk1-1* mutants treated with water (control) or 0.5 μg/μL poly(I:C). Inlays show enlargements of the areas within the dashed boxes. Scale bar, 10 μm. **E)** Mean callose content in PD determined in 9 leaf disks taken from 3 plants per treatment (dots). The total number of evaluated PD is given at the base of each column. Error bars show the SEM. One way ANOVA of the mean values ($P = <0.0001$) followed by Sidak's test for pairwise comparisons. ****, $P = < 0.0001$; ns = nonsignificant. The mean callose intensity levels indicate a drastic inhibition of the poly(I:C)-induced PD callose deposition response in *serk1* as compared to the WT.

(**Figure 2.** Continued)
callose deposition at PD is strongly reduced in the *bik1 pbl1* mutant. Images were taken 30 min after treatment and the WT control of the same experiments is shown in **C**). Inlays show enlargements of the areas within the dashed boxes. Scale bar, 20 μm. Mean callose content in PD determined in 3 leaf disks from 3 plants per treatment (dots). The total number of evaluated PD is given at the base of each column. Error bars show the SEM. Two-tailed *t*-test; ns, nonsignificant. **H)** Poly(I:C)-induced MPK activation is reduced in the *bik1 pbl1* mutant. Immunoblot detection of phosphorylated MPK. Samples were harvested 30 min after treatment with 0.5 μg/μL poly(I:C), 1 μM flg22, or water. "*bik1*" stands for *bik1 pbl1*. CBB, Coomassie Brilliant Blue-stained gel showing staining of ribulose-bisphosphate-carboxylase (Rubisco) as gel loading control. **I)** *bik1 pbl1* plants do not show significant seedling root growth inhibition in the presence of poly(I:C) as compared to WT Col-0 plants. Seedlings were kept for 12 d in 0.5 μg/μL poly(I:C) or water. Scale bar, 1 cm. Quantification of poly(I:C)-induced root growth inhibition in *A. thaliana* WT Col-0 and *bik1 pbl1* seedlings. Analysis of 6 to 7 seedlings (dots) per condition. Two-tailed Mann–Whitney test; ****, $P = < 0.0001$; ns, nonsignificant.

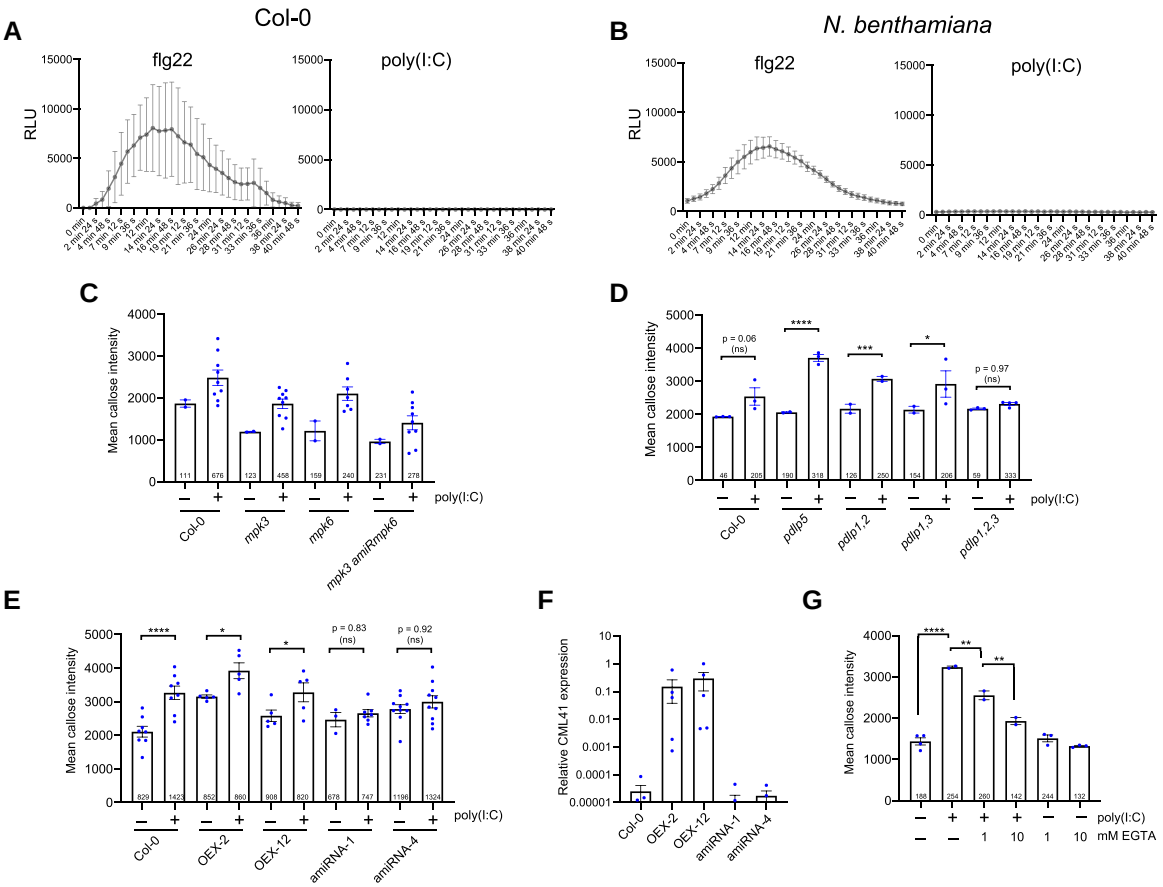

Figure 4. Poly(I:C)-induced PD callose deposition is ROS- and MPK3/6 cascade-independent but requires PDLP1/2/3 and CML41. **A and B)** Unlike flg22, poly(I:C) treatment does not induce any ROS production in Arabidopsis **A**) or *N. benthamiana* **B**). RLU, relative luminescence units. Mean values (dots) and error bars (standard deviation) obtained for each time point for 10 replicates (leaf disks) per treatment. **C)** Poly(I:C)-induced callose deposition at PD is not affected in *mpk3* and *mpk6* single mutants, and neither in a *mpk3* mutant in which *MPK6* is silenced by an artificial miRNA (*mpk3 amiRmpk6*). Mean callose content in PD 30 min after treatment with 0.5 μg/μL poly(I:C) or water and determined in 2 leaf disks from 2 control-treated plants of each genotype and 9 leaf disks from 3 poly(I:C)-treated plants for each genotype (dots). The total number of evaluated PD is given at the base of each column. Error bars show the SEM. The trends are unequivocal despite the absence of a statistical test (different sample numbers between control- and poly(I:C)-treated conditions). **D)** Poly(I:C)-induced callose deposition at PD is independent of PDLP5 but depends on the redundantly acting PDLP1, PDLP2, and PDLP3. Mean callose content in PD 30 min after treatment with 0.5 μg/μL poly(I:C) or water and determined in 3 (or 4) leaf disks from 3 (or 4) plants per treatment and genotype (dots). The total number of evaluated PD is given at the base of each column. Error bars show the SEM. One-way ANOVA of the mean values ($P = <0.0001$) followed by Sidak's test for pairwise comparisons. ****, $P = < 0.0001$; ***, $P = < 0.001$; *, $P = < 0.05$; ns = nonsignificant. **E and F)** Efficient poly(I:C)-induced callose deposition at PD depends on CML41. **E)** PD callose deposition levels in poly(I:C)-treated and control-treated leaf disks of 2 *CML41*-overexpressing lines (OEX2 and OEX12) and of 2 lines in which the expression of *CML41* is reduced by expression of artificial miRNA (amiRNA1 and amiRNA4). As compared to the WT (Col-0) and the *CML41*-overexpressing lines, the inducibility of PD callose deposition by poly(I:C) is strongly decreased in the amiRNA lines. Mean callose content in PD 30 min after treatment with 0.5 μg/μL poly(I:C) or water and determined in up to 9 leaf disks from 3 plants per treatment and genotype (dots). The total number of evaluated PD is given at the base of each column. Error bars show the SEM. One way ANOVA of the mean values ($P = <0.0001$) followed by Sidak's test for pairwise comparisons. ****, $P = < 0.0001$; *, $P = < 0.05$; ns = nonsignificant. **F)** Relative levels of *CML41* expression in plants of the OEX2, OEX12, amiRNA1, and amiRNA4 lines in comparison to WT (Col-0), as determined by RT-qPCR. Mean values and standard errors obtained by RT-qPCR with 3 to 6 biological replicates (dots). **G)** poly(I:C)-induced callose deposition is reduced in the presence of EGTA. Mean callose content in PD as determined in 3 Col-0 leaf disks per treatment (dots). The total number of evaluated PD is given at the base of each column. Error bars show the SEM. One-way ANOVA of the mean values ($P = <0.0001$) followed by Sidak's test for pairwise comparisons. ****$P = < 0.0001$; **$P = < 0.001$.

receptors for tubule-forming viruses (Amari et al. 2010). Whereas *pdlp1 pdlp2* (*pdlp1,2*) and *pdlp1 pdlp3* (*pdlp1,3*) double mutants showed a normal poly(I:C)-induced callose deposition, *pdlp1 pdlp2 pdlp3* (*pdlp1,2,3*) triple mutant plants were unable to significantly increase PD-associated callose levels in response to poly(I:C) (Fig. 4D). This observation suggests the involvement of PDLP1, PDLP2 and PDLP3 in dsRNA-triggered immunity and in mediating the callose deposition at the PD.

In further screening of other mutants for dsRNA sensitivity, we found that efficient poly(I:C)-induced callose

deposition at PD also depends on the Ca^{2+}-binding, PD-localized CALMODULIN-LIKE protein 41 (CML41). This protein was shown to mediate rapid callose deposition at PD associated with a decreased PD permeability following flg22 treatment (Xu et al. 2017). Plants of *CML41* overexpressing transgenic lines (*CML41-OEX-2* and *CML41-OEX-12*) (Xu et al. 2017) showed increased PD-associated callose levels upon poly(I:C) treatment similar to WT Col-0 plants (Fig. 4E). In contrast, transgenic plant lines in which *CML41* is downregulated by an artificial miRNA (*CML41-amiRNA-1* and *CML41-amiRNA-4*) (Xu et al. 2017) showed a 7- to 8-fold lower ability to respond to this treatment compared to WT Col-0 (Fig. 4E). The reduction in the response to poly(I:C) of *CML41-amiRNA* plants is consistent with the reduced level of *CML41* expression in these lines (Xu et al. 2017) (Fig. 4F).

In agreement with the role of CML41 in the callose deposition response to poly(I:C), the permeability of PD was previously shown to be sensitive to cytosolic Ca^{2+} concentrations (Tucker and Boss 1996; Holdaway-Clarke et al. 2000). To test the role of Ca^{2+} in dsRNA-triggered innate immunity, we treated plants with poly(I:C) together with EGTA, a Ca^{2+}-chelating molecule. The level of callose induced at PD after dsRNA treatment was reduced in the presence of EGTA in a concentration-dependent manner (Fig. 4G), indicating a role of Ca^{2+} in poly(I:C)-triggered PD regulation. Together, these results suggest a role for CML41 and Ca^{2+} in the poly(I:C)-induced defense response at PD. The observation that the poly(I:C)-induced callose levels were not significantly increased by *CML41* overexpression may be due to that the endogenous level of *CML41* expression in WT plants is sufficient for the full activity of the PD-localized CML41 proteins. However, the level of expression in WT plants is critical as a reduction in *CML41* levels strongly affected PD callose levels.

BIK1/PBL1 and CML41 are essential for dsRNA-induced antiviral resistance

Previously, we showed that poly(I:C) cotreatment during virus inoculation protects Arabidopsis plants against infection by oilseed rape mosaic virus (ORMV) and that efficient protection depends on SERK1 (Niehl et al. 2016). As we demonstrate here, SERK1 plays an essential role in the poly(I:C)-induced callose deposition at PD, implying a role of PD closure in dsRNA-induced antiviral resistance. To further test the significance of PD callose deposition of BIK1/PBL1 and CML41 in dsRNA-induced antiviral resistance, we inoculated poly(I:C)-treated and nontreated *bik1 pbl1* and *CML41 amiRNA-1* plants with ORMV. Whereas poly(I:C) treatment prevented symptoms at 28 dpi and resulted in a strongly reduced virus titer in WT Col-0 plants, *bik1 pbl1* and *CML41 amiRNA-1* plants showed severe virus-infected symptoms and accumulated high virus levels in poly(I:C)-treated plants similar to those plants without poly(I:C) treatment upon ORMV infection (Fig. 5, A and B). Ablation of virus-inoculated leaves from plants at different times after inoculation showed that the time required for the virus to exit the inoculated leaf and to cause systemic infection was 3 d in WT plants. By contrast, this time was reduced to 24 h in *bik1 pbl1* mutants and *CMLl41-amiRNA-1* plants (Fig. 5, C and D). These findings show that dsRNA-induced antiviral PTI occurs at the level of virus movement. Consistent with this PTI effect on virus movement, the experiments reveal a dsRNA-induced signaling pathway that requires SERK1, BIK1/PBL1, CML41, Ca^{2+} and PDLP1/2/3 for callose deposition at PD. This dsRNA-induced callose deposition at PD is likely independent of ROS and MPK3/6 signaling, which differs from the immune signaling triggered by fungal and bacterial elicitors (Kadota et al. 2014; Cheval et al. 2020).

dsRNA-induced callose deposition is suppressed by viral MP

The plant-pathogen arms race causes pathogens to evolve virulent effectors that overcome host defenses. Viral MPs are essential for mediating virus movement during infection. We tested whether viral MPs are involved in the suppression of the dsRNA-induced callose deposition at PD. To address this question, we divided the local TMV infection site into different zones (Fig. 6A): zone I ahead of infection and without MP, zone II at the virus front where MP facilitates virus movement, zone III behind the infection front, and zone IV, which is the center of the infection site where MP is no longer expressed. *In vivo* detection of dsRNA with GFP-fused dsRNA-binding protein B2 of Flock house virus (Monsion et al. 2018) shows that zones II-IV accumulate dsRNA in distinct replication complexes that also produce MP (Fig. 6B). Aniline blue staining demonstrates high PD-associated callose levels within and around the infection site (Fig. 6C). However, cells in zone II and zone III, where virus cell-to-cell movement is associated with a transient activity of MP in increasing the PD size exclusion limit (SEL) (Oparka et al. 1997), exhibit a marked reduction in PD-associated callose levels as compared to cells in zone I (ahead of infection) and zone IV (center of infection) (Fig. 6, C and D). The low level of PD-associated callose in cells at the virus front (zone II) is consistent with the ability of MP to interfere with dsRNA-triggered immunity leading to PD closure.

To test this hypothesis, we examined whether the expression of MP causes suppression of the poly(I:C)-induced callose deposition at PD in the absence of viral infection. Transgenic *N. benthamiana* plants that stably express MP:RFP at PD (Fig. 7, A and B) complement a MP-deficient TMV mutant for movement, thus indicating that the MP:RFP in these plants is functional (Fig. 7C). Treatment of such plants with poly(I:C) led to a significantly lower induction of callose deposition at PD as compared to WT plants (Fig. 7, D to F). The ability of poly(I:C) treatment to induce callose deposition at PD was also reduced upon transient expression of MP:GFP (Fig. 7, G to I).

Importantly, the same effect was observed with MP^{C55}:GFP. This mutant MP lacks 55 amino acids from the C-terminus but still accumulates at PD and is functional in TMV movement (Boyko et al. 2000). By contrast, dysfunctional MP^{P81S} carrying a P to S substitution at amino acid position 81, which fails to

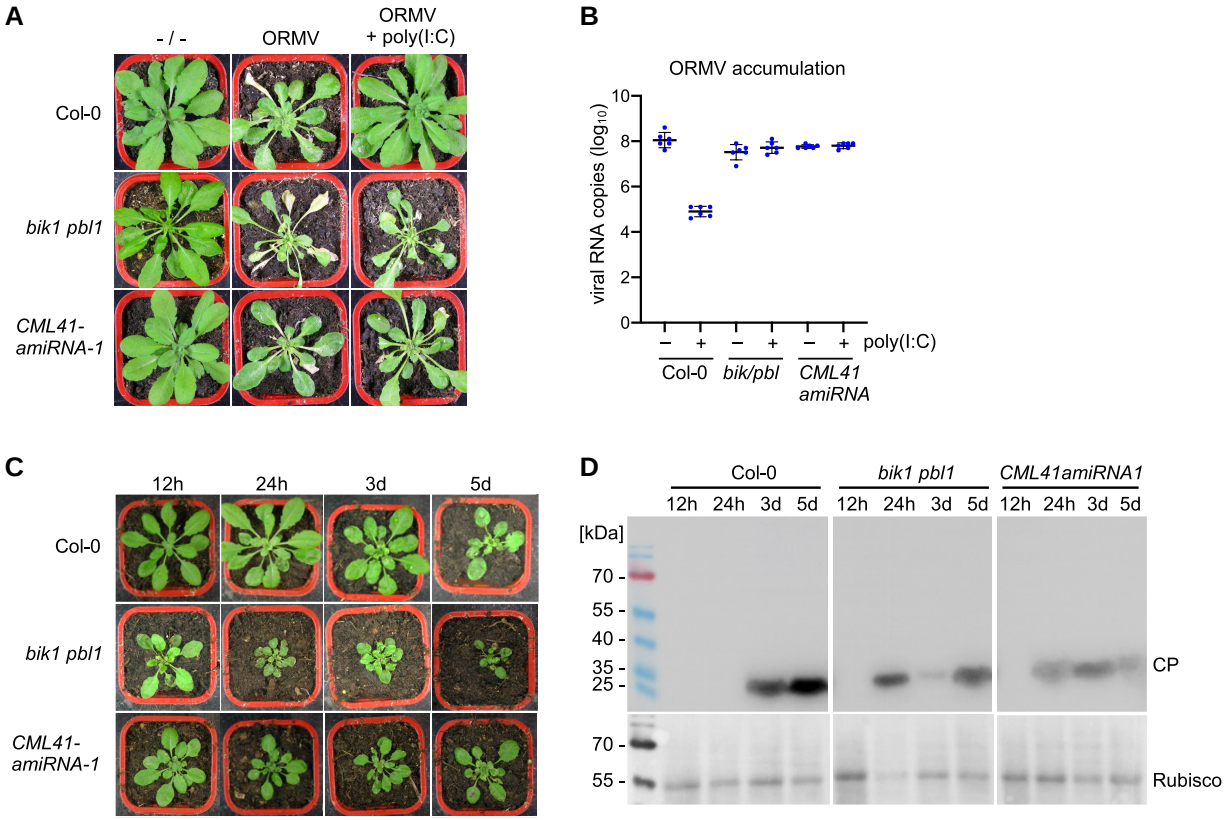

Figure 5. BIK1/PBL1 and CML41 are required for antiviral defense. **A and B**) disease symptoms (A) and viral RNA accumulation (B) at 28 dpi in wild-type plants and mutants inoculated with ORMV in the presence and absence of 0.5 μg/μL poly(I:C). Unlike in wild-type plants (Col-0) the antiviral effect of poly(I:C) treatment is lost in *bik1 pbl1* mutants and *CML41-amiRNA-1* expressing plants. Viral RNA accumulation (B) is depicted for 6 biological replicates per condition. Mean values and standard errors are shown. **C and D)** BIK1 and CML41 inhibit virus movement. **C)** Representative symptom phenotypes at 21 dpi of Arabidopsis Col-0 plants, *bik1 pbl1* mutant plants and plants transgenic for *CML41-amiRNA-1* that were locally inoculated with ORMV and from which the inoculated leaves were removed at the indicated times in hours (h) and days (d). Whereas systemic leaves of Col-0 plants show symptoms on plants that carried the inoculated leaves for 3 or more days following inoculation, the systemic leaves of the *bik1 pbl1* mutant and of the CML41-amiRNA-expressing plants show symptoms already if the inoculated leaves were present for only 24 h. **D)** Immunoblot analysis of the youngest systemic leaves at 21 dpi using antibodies against viral coat protein (CP) (youcai mosaic virus antibody, AS-0527, DSMZ, Braunschweig, Germany). The pattern of CP expression in the systemic leaves confirms that in WT Col-0 plants the virus needs between 24 h and 3 d to exit the inoculated leaves and move systemically, whereas the time needed for systemic movement is reduced to less than 24 h in the *bik1 pbl1* mutant and of the CML41-amiRNA expressing plants, thus indicating a role of BIK1 and CML41 in restricting virus movement.

target PD and to support virus movement (Boyko et al. 2002), did not interfere with poly(I:C)-induced callose deposition. These experiments show that the TMV MP can significantly interfere with the dsRNA-induced callose deposition at PD, and that this interference correlates with MP activity in virus movement. Consistent with the absence of a significant role of MPK3/6 signaling in poly(I:C) induced callose deposition, expression of MP:GFP or the MP:GFP mutants did not interfere with flg22 elicitor-triggered MPK activation (Fig. 7J). Interestingly, MP does not reduce PD callose deposition induced by flg22 (Fig. 7, K and L), suggesting that MP interferes with signaling or signaling target mechanisms that are different between both elicitors.

To determine if also the MPs of other viruses interfere with the poly(I:C) induction of PD callose deposition, we tested the MPs of ORMV and Turnip vein clearing virus (TVCV). The RFP-fused version of these MPs and the MP of TMV are functional as their transient expression in *N. benthamiana* leaves allowed the intercellular spreading of the coexpressed, MP-deficient TMVΔMΔC-GFP replicon, as can be seen by the development of multiple fluorescent foci (Fig. 8A). Consistent with function, the different MP:RFP fusion proteins colocalize with PD-associated callose (Fig. 8B). Importantly, similar to the functional MP:RFP derived from TMV, the functional MP:RFP fusion proteins derived from ORMV and TVCV strongly reduced the levels of PD callose deposition induced by poly(I:C) treatment (Fig. 8, C and D). Thus, the capacity to interfere with poly(I:C)-induced PD callose deposition may be a widespread function of viral MPs to achieve efficient infections. These observations also further substantiate the importance of antiviral PTI in the inhibition of virus movement for plants to fend off virus infections.

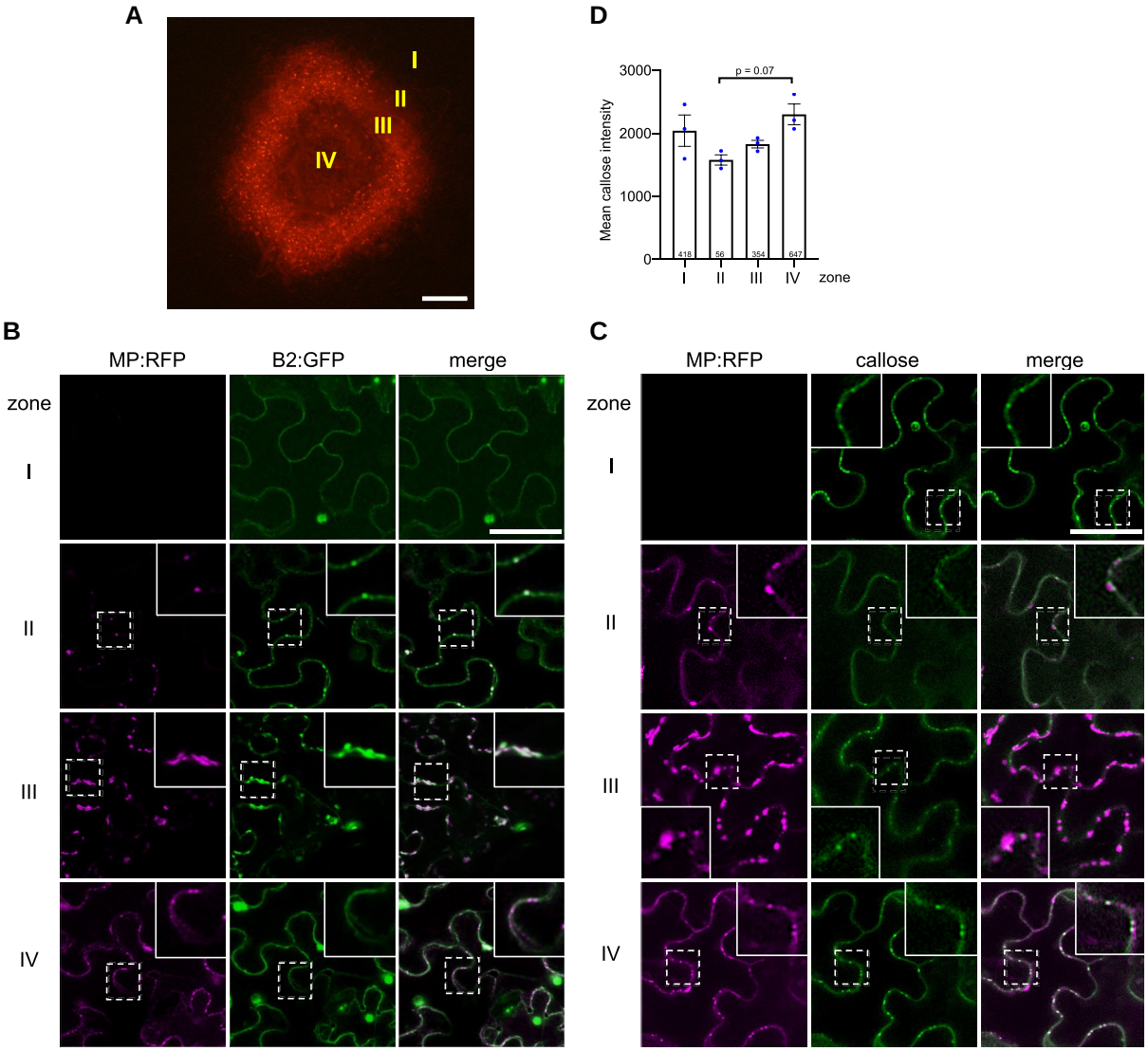

Figure 6. Viral MP expression correlates with a suppression of PD-associated callose levels. **A)** The local site of infection by TMV-MP:RFP (at 4 dpi) in *N. benthamiana*. Different zones ahead of infection (zone I), at the infection front (zone II), behind the infection front (zone III), and in the center of infection (zone IV) are indicated. Scale bar, 200 μm. **B)** Viral dsRNA accumulation in the different zones of local TMV infection. Inlay images show magnifications of image areas framed by a dashed line. Scale bar, 20 μm. The MP of TMV is tagged with RFP (MP:RFP), and the accumulating dsRNA is imaged through the binding of the *Flock house virus* B2 protein fused to GFP (B2:GFP). In cells of zone I (noninfected cells ahead of infection), B2:GFP shows a nucleo-cytoplasmic distribution, which is the typical distribution of this protein in the absence of dsRNA (Monsion et al. 2018). In cells at the virus front (zone II), B2:GFP colocalizes to MP:RFP to spots at the cell wall (likely at PD), indicating the localization of early VRCs engaged in virus replication and virus movement. In zone III, the VRCs have grown in size and accumulate high amounts of dsRNA consistent with high levels of virus replication to produce virus progeny. In zone IV, the MP is no longer expressed, but residual MP:RFP is still seen in PD. The B2:GFP-tagged VRCs now appear rounded. **C)** The pattern of MP:RFP and callose accumulation in the different zones. Inlays show magnifications of the image areas highlighted by dashed boxes. Scale bar, 40 μm. In zone II, where MP localizes to PD to facilitate virus movement, and to some extend also still in zone III, the PD-associated callose levels are decreased as compared to the other zones. **D)** Mean callose content of PD in the different zones of 3 different infection sites (dots). The total number of evaluated PD is given at the base of each column. Error bars show the SEM. One way ANOVA of the mean values ($P = 0.0581$) followed by Sidak's test for pairwise comparison.

Poly(I:C) may enter plant cells

As viruses replicate and produce dsRNA within cells, poly (I:C)-induced responses may only be relevant to virus infection if poly(I:C) is able to enter cells. To test this, we used B2:GFP as an intracellular dsRNA localization marker and monitored the responses of B2:GFP-transgenic *N. benthamiana* plants upon poly(I:C) treatment. Externally applied poly(I:C) may enter cells from all sides and then diffuse into the cytoplasm. Thus, a strong redistribution of B2:GFP similar as in virus-infected cells, where dsRNA production centers within the viral replication complexes (VRCs), should not be expected. Nevertheless, as compared to control-treated tissues,

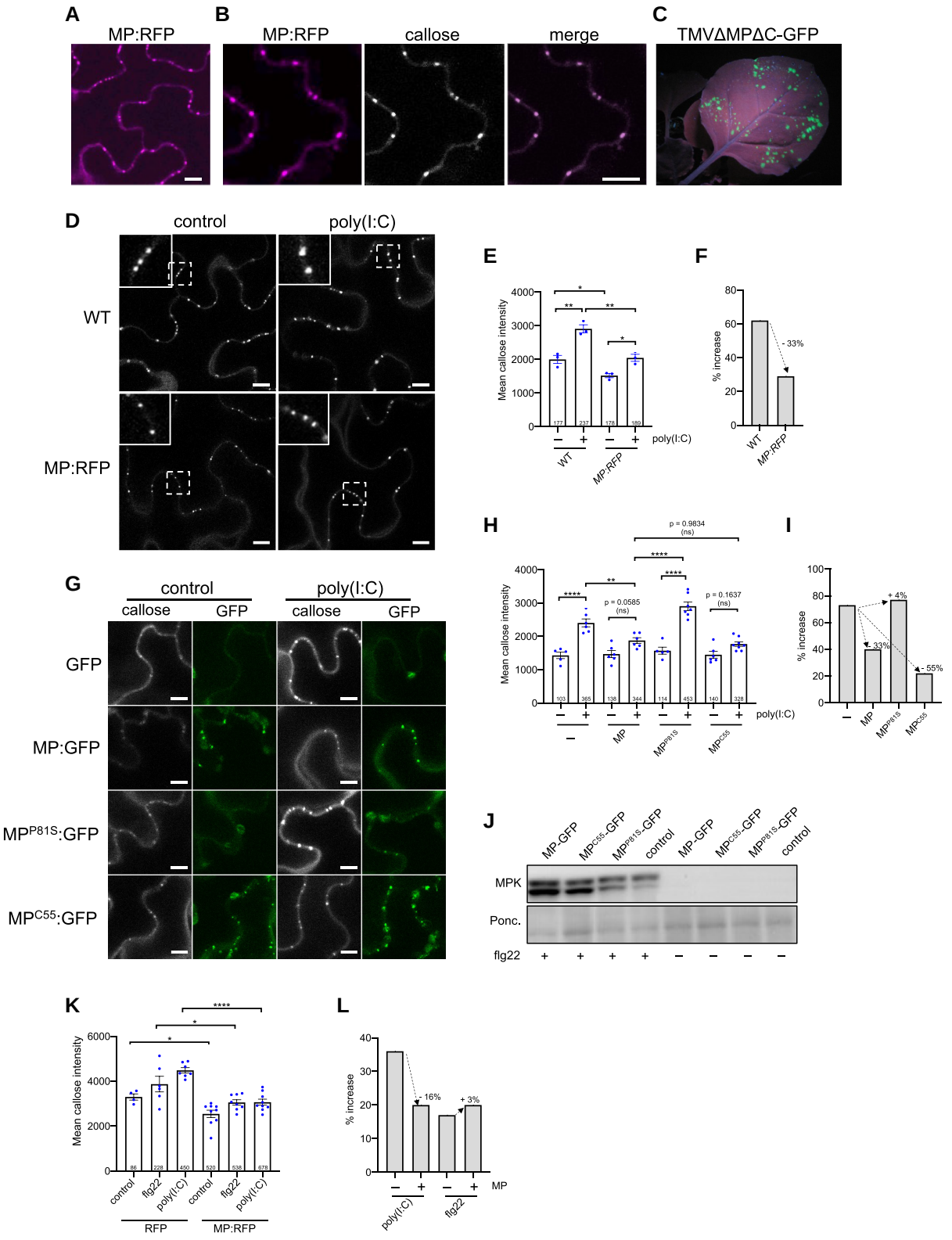

Figure 7. Suppression of poly(I:C)-induced immunity by MP. **A to F)** Inhibition of dsRNA-induced callose deposition in MP:RFP-transgenic *N. benthamiana* plants. **A to C)** MP:RFP is functional. **A)** Transgenically expressed MP:RFP localizes to distinct locations at the cell wall. Scale bar, 10 μm. **B)** The MP:RFP localizes to PD as revealed by callose staining with aniline blue. Scale bar, 10 μm. **C)** The stably expressed MP:RFP in this line is functional and complements infection upon inoculation with in vitro transcribed infectious RNA of the MP-deficient TMVΔMΔC-GFP (Vogler et al. 2008), as can be seen by the occurrence of distinct GFP fluorescent infection sites at 7 dpi. **D** to **F**) Inhibition of dsRNA-induced callose deposition in MP:RFP-transgenic plants. **D)** Leaf epidermal cells of nontransgenic (WT) and MP:RFP-transgenic *N. benthamiana* plants treated or

(continued)

poly(I:C)-treated tissues exhibited a significant decrease in the level of B2:GFP in the nucleus (Fig. 9, A to D). Moreover, a slight but significant increase in B2:GFP fluorescence levels in the cytoplasm was noted at later time points (Fig. 9, E and F). These observations are consistent with a redistribution of B2:GFP in poly(I:C) treated cells, thus suggesting poly(I:C) uptake.

Discussion

dsRNA-induced callose deposition during virus infection

Accumulation and degradation of callose at PD play an essential role in controlling macromolecular transport between cells (De Storme and Geelen 2014; Wu et al. 2018). Mutations and conditions that alter the levels of callose at PD strongly affect the conductivity of PD for macromolecular transport (Simpson et al. 2009; Guseman et al. 2010; Vatén et al. 2011; Benitez-Alfonso et al. 2013). A role of callose in plant-virus interactions became apparent from the observation that elevated callose levels in plants silenced for the callose-degrading enzyme restricted the spread of virus infection, thus suggesting that PD callose deposition may be part of early defense responses against virus attack (Beffa et al. 1996). However, how viruses trigger PD callose deposition and yet still maintain their cell-to-cell movement despite this host defense response remained open. The induction of callose deposition at PD by cell-autonomous replication of an MP-deficient TMV replicon led to the conclusion that virus replication induces "stress" leading to callose deposition at PD (Guenoune-Gelbart et al. 2008), but the nature of the "stress" and the underlying mechanism remained obscure. The finding that viruses induce innate immunity (Kørner et al. 2013) and that dsRNA is a potent PAMP elicitor in plants (Niehl et al. 2016) suggests dsRNA as a potential candidate for the perceived stress signal. Our data shown here that dsRNA-induced immunity is linked to PD callose deposition raise a model that virus replication causes callose deposition and PD closure mediated through a PTI response triggered by viral dsRNA.

MP facilitates virus movement by suppressing a dsRNA-induced PTI response

Because virus movement depends on prior replication of the viral genome (Christensen et al. 2009), and given that the virus must continue to replicate to produce progeny, the PTI response is likely triggered immediately in the newly infected cells at the infection front and maintained in cells behind the front. Thus, the perception of dsRNA may target PD for closure throughout the infection site. This mechanism may have evolved to isolate the infected cells from surrounding cells to prevent further spread of infection but also to protect the virus replication and virus progeny production in the infected cells against intercellular defense signaling. At the infection front, the dsRNA-producing virus must nevertheless be able to overcome PD closure in order to spread infection into noninfected cells. Consistently, pioneering studies with TMV showed that the virus moves between cells with the help of virus-encoded MP, that MP targets PD,

(**Figure 7.** Continued)
nontreated with poly(I:C) and stained with aniline blue. Inlay images show magnifications of image areas framed by a dashed line. Scale bar, 10 μm. Treatment of leaf tissues with 0.5 μg/μL poly(I:C) for 30 min causes a stronger increase in the level of PD-associated callose in WT plants than in MP:RFP-transgenic plants. **E)** Quantification of callose in leaf epidermal cells upon aniline blue staining. Mean callose content in PD determined in 3 leaf disks from 3 plants per treatment (dots). The total number of evaluated PD is given at the base of each column. Error bars show the SEM. One way ANOVA of the mean values ($P = <0.0001$) followed by Sidak's test for pairwise comparisons. $^{**}P = < 0.01$; $^{*}P = < 0.05$. **F)** Relative increase in median PD callose deposition in poly(I:C)-treated tissue compared to control-treated tissue (%) in WT and MP:RFP-transgenic plants. **G** to **I**) Inhibition of poly(I:C)-induced PD callose deposition by transiently expressed MP:GFP. Leaf disks excised from the GFP, MP:GFP, MP^{P81S}:GFP or MP^{C55}:GFP-expressing leaves 48 h after agroinfiltration were incubated for 1 d in water, then transferred into aniline blue solution with and without 0.5 μg/μL poly(I:C) and imaged after 30 min. **G)** Images of leaf epidermal cells stained for callose with aniline blue (callose) together with corresponding images of the same cell area showing GFP fluorescence. The ability of MP:GFP to reduce the poly(I:C) induction of callose deposition at PD is inhibited by a single amino acid exchange mutation in MP (P81S) previously shown to affect its ability to efficiently target PD and to function in virus movement. Functional MP with a C-terminal deletion of 55 amino acids (C55) but still targeting the PD inhibits poly(I:C)-induced callose deposition like wildtype MP. **H)** Quantification of mean PD-associated callose levels in leaf epidermal cells upon aniline blue staining. Several leaf disks from 3 plants per condition were analyzed and the total number of evaluated PD is given at the base of each column. Error bars show the SEM. One-way ANOVA of the mean values ($P = <0.0001$) followed by Sidak's test for pairwise comparisons. $^{****}P = < 0.0001$; $^{**}P = < 0.01$; ns = nonsignificant. **I)** Relative increase in median PD callose deposition in poly(I:C)-treated tissue as compared to control-treated tissue (%) in the presence of MP or MP mutants. Unlike functional MP and MP^{C55}, dysfunctional MP^{P81S} is not able to reduce the poly(I:C)-induced callose deposition. **J)** Immunoblot showing that the expression of wild type or mutant MP:GFP does not interfere with flg22-induced MPK activation. Ponc., Ponceau S-stained immunoblot membrane. **K)** flg22- and poly(I:C)-induced mean PD callose deposition in the presence of MP:RFP or RFP as control. Leaf disks excised from the RFP or MP:RFP-expressing leaves 48 h after agroinfiltration were incubated for 1 d in water, then transferred into aniline blue solution with and without 0.5 μg/μL poly(I:C) and imaged after 30 min. Several leaf disks from 2 plants were evaluated for each condition (dots) and the total number of evaluated PD is given at the base of each column. Error bars show the SEM. One-way ANOVA of the mean values ($P = <0.0001$) followed by Sidak's test for pairwise comparisons. $^{****}P = < 0.0001$; $^{*}P = < 0.05$. **L)** Relative increase in median PD callose levels in poly(I:C)-treated or flg22-treated tissue as compared to control-treated tissue (%) in the presence of MP:RFP (+) or RFP as control (−). Expression of MP:RFP reduced the poly(I:C)- but not the flg22-induced callose deposition.

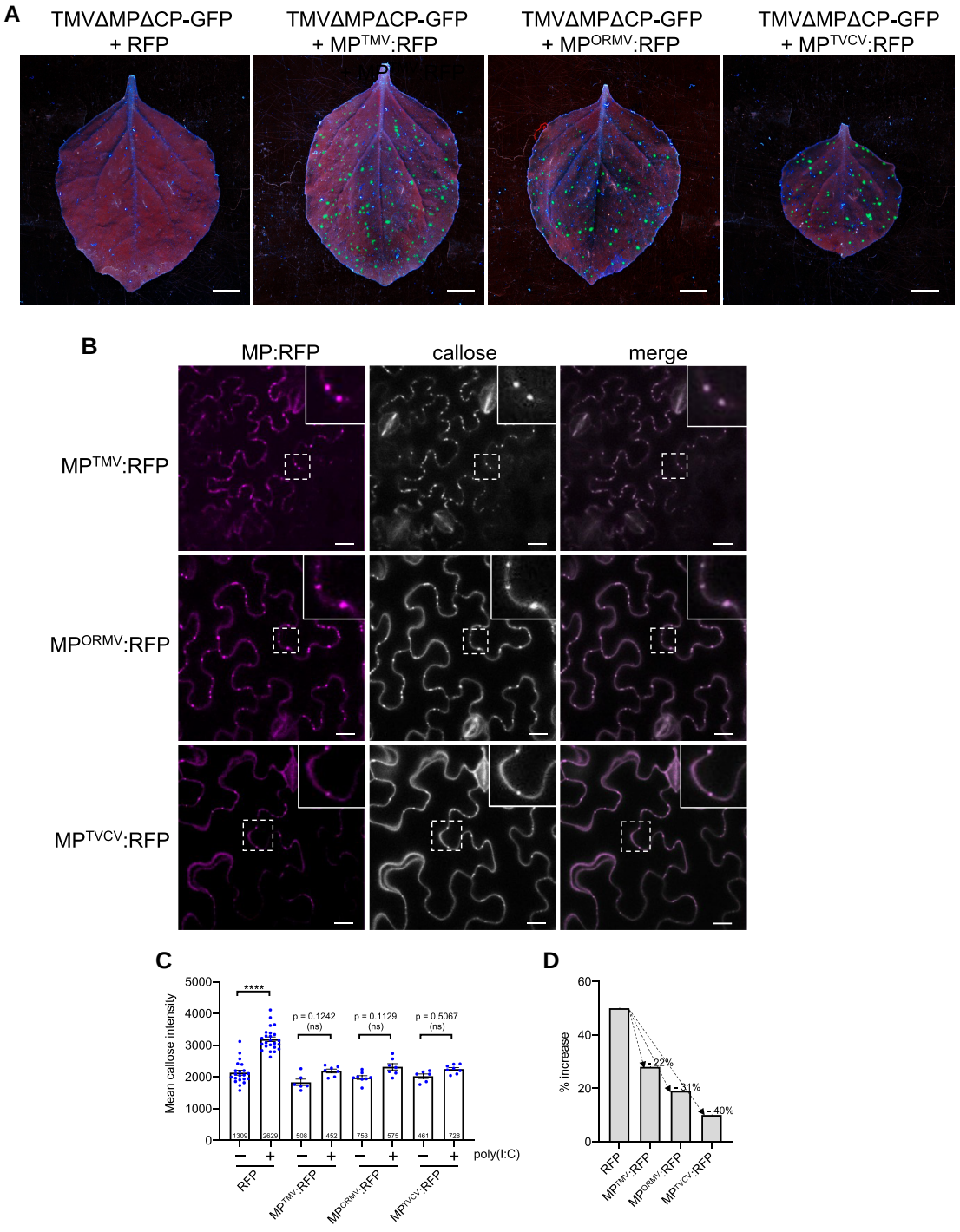

Figure 8. Inhibition of poly(I:C)-induced callose deposition by MPs of different viruses. **A)** Different MPs are functional. Unlike free RFP, RFP fusions to the MPs of TMV (MP^{TMV}:RFP), ORMV (MP^{ORMV}:RFP), and TVCV (MP^{TVCV}:RFP) complement the movement function of MP-deficient TMVΔM-GFP in *N. benthamiana*. Leaves were coinfiltrated with agrobacteria containing the respective RFP or MP:RFP-encoding plasmids together with highly diluted agrobacteria ($OD_{600\ nm} = 1 \times 10^{-5}$) for agro-inoculation with TMVΔMPΔCP-GFP. Pictures were taken at 5 dpi. Scale bar, 1 cm. **B)** MP^{TMV}:RFP, MP^{ORMV}:RFP, and MP^{TVCV}:RFP localize to PD as shown by the presence of callose. MP-expressing leaves were stained with aniline blue and imaged after 30 min. Inlay images show magnifications of image areas framed by a dashed line. Scale bar, 20 μm. **C and D)** Expression of either MP^{TMV}:RFP, MP^{ORMV}:RFP, or MP^{TVCV}:RFP strongly reduces the induction of PD callose deposition in the presence of poly(I:C). Leaf disks excised from the RFP (control) or MP:RFP-expressing leaves 48 h after agroinfiltration were incubated for 1 d in water, then transferred into aniline blue solution with and without 0.5 μg/μL poly(I:C) and imaged after 30 min. **C)** Mean callose content in PD of poly(I:C)-treated and control-treated

(continued)

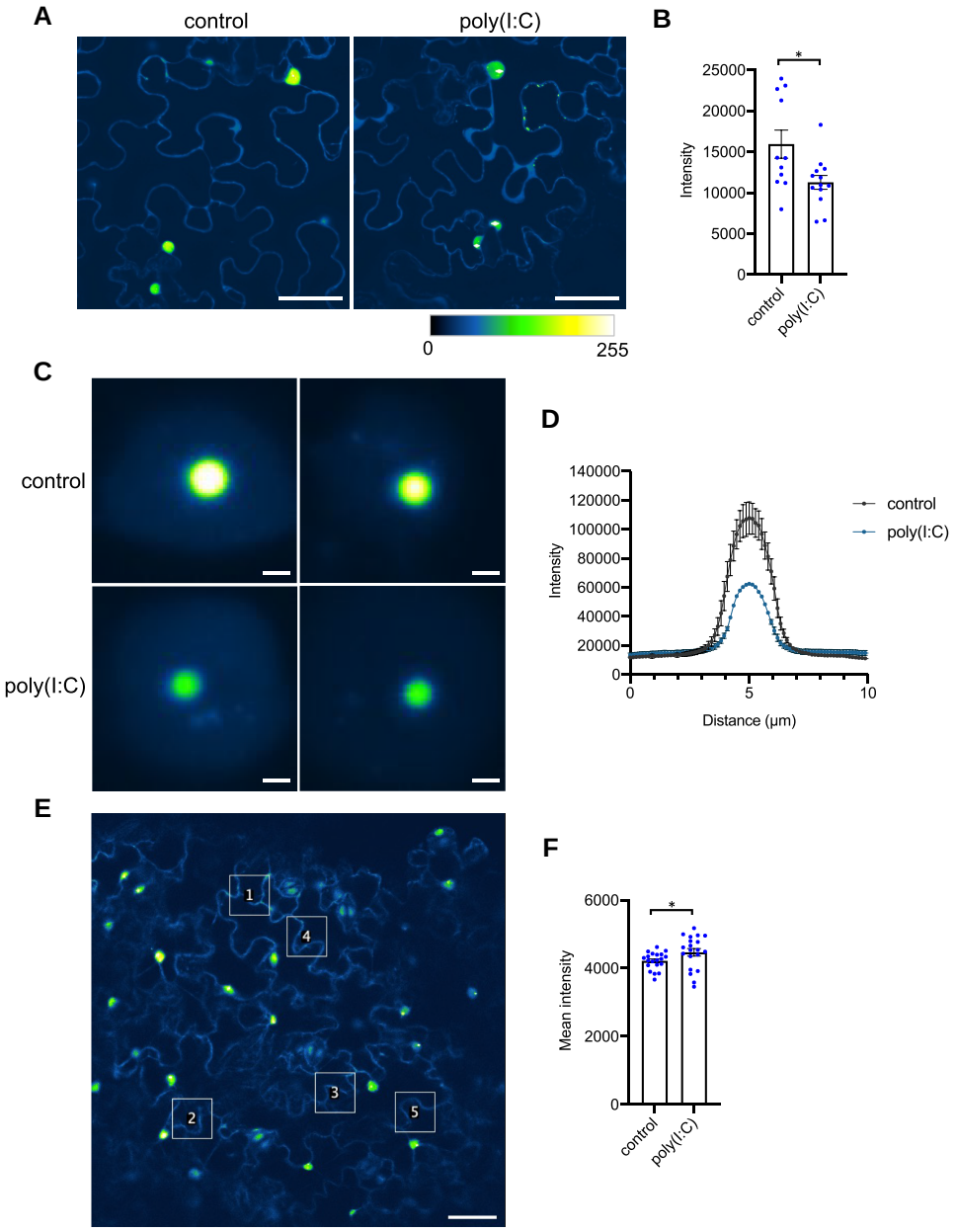

Figure 9. Poly(I:C) treatment causes redistribution of the dsRNA-binding protein B2. B2:GFP-transgenic *N. benthamiana* leaf tissue treated with water (control) or 0.5 μg/μL poly(I:C) for at least 1 h and imaged with the ImageJ "green fire blue" color look-up table (LUT). **A** to **D**) Poly(I:C) treatment reduces the level of B2:GFP fluorescence in the nuclei. **A)** Nucleo-cytoplasmic distribution of B2:GFP in poly(I:C) treated and control tissues. Scale bar, 50 μm. **B)** Reduction of nuclear B2:GFP fluorescence 1 h after poly(I:C) treatment. Mean fluorescence intensity of nuclei in 3 to 4 images analyzed per treatment. Two-tailed *t*-test; *, $P = <0.05$. **C)** Representative images of individual nuclei in poly(I:C) and control-treated tissue. Scale bar, 2 μm. **D)** Mean B2-GFP fluorescence intensity profile along lines (10 μM) drawn across the nuclei of poly(I:C) and control-treated tissues. Three nuclei were analyzed per treatment. **E** and **F)** Poly(I:C) treatment causes slight increases in B2:GFP fluorescence in the cytoplasm. **E)** B2:GFP fluorescence was measured by randomly selecting 5 square ROIs per image 15 h after treatment. Scale bar, 50 μm. **F)** B2:GFP fluorescence intensity in the cytoplasm is increased upon poly(I:C) treatment. Four images were analyzed per treatment. Two-tailed *t*-test; $^*P = <0.05$.

(**Figure 8.** Continued)
tissue. For each treatment, several leaf disks from 3 plants were analyzed for PD-associated callose levels. RFP data are combined data from the leaf disks that were used as RFP control in the individual agroinfiltration experiments. The total number of evaluated PD is given at the base of each column. Error bars show the SEM. One-way ANOVA of the mean values ($P = <0.0001$) followed by Sidak's test for pairwise comparisons. **D)** Relative increase in median PD callose deposition in poly(I:C)-treated tissue as compared to control-treated tissue (%) in the presence of the different RFP-fused MPs or RFP as control. $^{****}P = < 0.0001$; ns = nonsignificant.

and that it increases the SEL of PD and thus the permeability of the channels for macromolecular trafficking (Citovsky 1999). Importantly, using microinjection, MP was shown to gate the PD between cells only at, but not behind, the virus infection front (Oparka et al. 1997). Our observations link this activity to the suppression of a dsRNA- induced response by showing (i) that cells at the virus infection front, where MP increases the PD SEL, have a significantly lower level of callose at PD as compared to other cells and (ii) that the induction of PD callose deposition by dsRNA [poly(I:C)] is significantly reduced by ectopically expressed MP. The ability of MP of TMV to interfere with dsRNA-induced callose deposition seems to reflect an activity shared with other MPs as similar to MP^{TMV} also the expression of MP^{ORMV} or MP^{TVCV} reduced the intensity of PD callose induction by poly(I:C) as compared to the control (absence of the respective MP) (Fig. 8). These observations suggest a paradigm for virus movement whereby dsRNA produced by TMV replication in a newly infected cell at the infection front triggers a host PTI response that targets PD for callose deposition and closure in order to restrict the spreading of the virus. To allow the spread of replicated viral genomes into noninfected cells, the viral MP acts as an effector to transiently suppress this dsRNA-induced response (Fig. 10, A and B). As dsRNA-induced immunity mainly restricts the viral cell-to-cell movement but does not affect much on virus replication in the infected cells, and viral MP overcomes this layer of immunity by inhibiting virus movement through PD, the virus accumulates in systemically infected plants of *bik1/pbl1* and *cml41amiRNA* lines to a similar level as in wild type plants (Fig. 5B). However, upon elicitation of the poly(I:C)-mediated PTI response, the virus-encoded MP may become insufficient for efficient suppression, thus leading to the inhibition of virus movement (Figs. 1, A and B and 5, C and D) and delayed accumulation in the infected plants (Fig. 5B). Additionally, the BIK1 family RLCKs play redundant roles in PTI signaling against bacterial infection (Rao et al. 2018). It is possible that additional members of RLCKs may also be involved in the antiviral immunity.

The MP is expressed in cells at and closely behind the infection front (Fig. 6, A to C). The restriction of MP activity

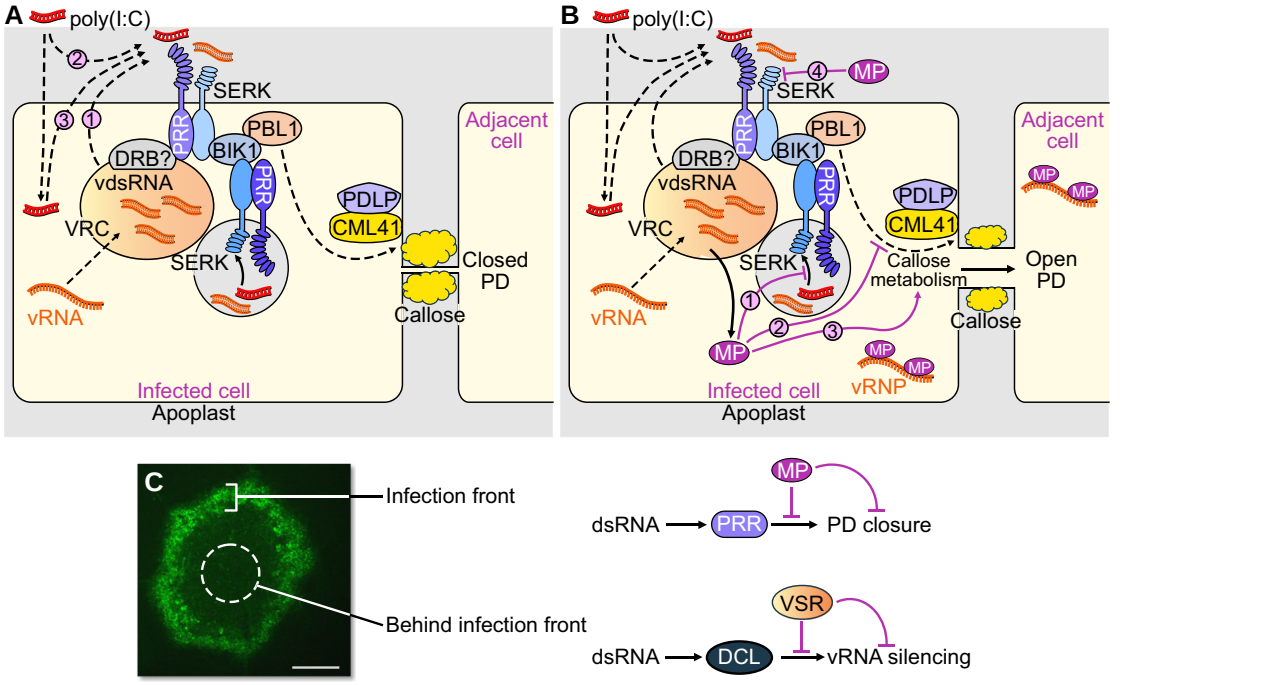

Figure 10. Virus infection facilitated by virus-encoded effector proteins. **A** and **B)** Suppression of PTI by MP. **A)** Perception of dsRNA produced in cortical ER-associated VRCs at the PM by an unknown membrane-associated or intracellular PRR and the SERK1 coreceptor (with potential contribution by one or more other coreceptors) triggers a signaling pathway leading to callose deposition and PD closure. dsRNA produced during infection in the VRC may require secretion into the apoplasm (1) to allow perception at the PM. Externally applied poly(I:C) may be perceived from the apoplasm (2) or secreted upon initial uptake by the cells (3). Viral dsRNA as well as poly(I:C) may also be sensed by an intracellular cytoplasmic PRR, or by an internalized SERK–PRR complex, as shown in the figure in endosomes, shown as a gray vesicle. **B)** MP suppresses dsRNA-triggered callose deposition and allows intercellular spread of the viral ribonucleoprotein complex (vRNP). The MP may inhibit dsRNA sensing by the intracellular dsRNA receptor or internalized SERK-PRR complex (1), interact with intracellular PTI signaling (2) or modify the activity of callose synthesizing or degrading enzymes at PD (3). The MP may also be secreted to inhibit dsRNA perception at the PM (4). **C)** dsRNA triggers PTI and antiviral RNA silencing and both responses are suppressed by viral effector proteins to support virus propagation. Whereas MP acts in cells at the virus front to facilitate virus movement by blocking a dsRNA-induced callose defense response at PD, the VSR blocks dsRNA-induced antiviral RNA silencing in the center of infection sites to support virus replication and production of virus progeny. A local infection site of TMV encoding MP fused to GFP (TMV-MP:GFP, 7 dpi) in *N. benthamiana* is shown. Scale bar, 1 mm.

and of low callose levels in cells at the infection front indicates that the protein exists in different activity states. Consistently, several studies correlated the activity of MP with its phosphorylation state (Lee and Lucas 2001). The partial, rather than full, suppression of dsRNA-induced callose deposition by ectopically expressed MP may reflect the different activity states of MP expressed under such conditions.

The mechanism by which MP suppresses the dsRNA-induced callose deposition at PD remains to be studied. dsRNA sequestration by MP is precluded as MP has no dsRNA binding activity (Citovsky et al. 1990). Electron micrographs indicated that the TMV MP forms fibrillar substructures within PD cavities (Ding et al. 1992; Moore et al. 1992; Heinlein et al. 1998), but it is unknown whether these structures are functional. Several studies support the hypothesis that a callose-degrading beta-1,3-glucanase enzyme activity may regulate virus movement (Iglesias and Meins 2000; Bucher et al. 2001; Levy et al. 2007), but strong evidence indicating that viruses like TMV indeed operate such activities for virus movement is lacking. More recent observations suggest that the MPs of different viruses interact with the synaptotagmin SYTA for movement (Uchiyama et al. 2014; Levy et al. 2015; Yuan et al. 2018). Synaptotagmins (SYTs) and other Ca^{2+}-sensitive C2 domain-containing proteins, such as the multiple C2 domains and transmembrane region proteins (MCTPs) are proposed to function as membrane-tethering proteins at membrane contact sites (Tilsner et al. 2016; Brault et al. 2019). Notably, the strand of endoplasmic reticulum (desmotubule) that traverses the PD channel between cells is tethered to the adjacent plasma membrane (PM) by MCTPs and SYTs (Brault et al. 2019; Ishikawa et al. 2020). Therefore, it is conceivable that MPs target SYTA to reach PD or even to modify a membrane tethering activity of SYTA within PD in order to alter the cytoplasmic space between the tethered membranes available for macromolecular transport (Pitzalis and Heinlein 2017). However, while further studies are needed to explore this idea, the results shown here promote the model that the MPs of TMV and also the MPs of ORMV and TVCV facilitate movement by interacting with components of the dsRNA-induced signaling and callose synthesis and turnover pathways to inhibit callose deposition at PD. The MPs may interfere with these pathways in the cytoplasm or at PD (Fig. 10, A and B). However, earlier studies indicated that the MPs of TMV, TVCV and cauliflower mosaic virus have the capacity to interact with the cell wall protein pectin-methylesterase (PME) which may allow transport of MP through the secretory pathway (Chen et al. 2000). It is conceivable, therefore, that MPs are partially secreted to inhibit the activity of the dsRNA perceiving receptors at the PM (Fig. 10B). However, whether the MPs of TMV, ORMV, and TVCV inhibit PD callose deposition through interaction with PTI signaling components or rather through direct interactions with callose synthesizing or degrading enzymes at PD remain to be investigated. As the MP of TMV suppressed PD callose deposition triggered by either poly(I:C) but not by flg22, the signaling components, enzymes, or mechanisms affected by MP may differ between poly(I:C)- and flg22- triggered pathways.

dsRNA induces antiviral defense through a novel PTI signaling pathway

We have shown here that the dsRNA-induced signaling pathway leading to callose deposition at PD involves SERK1, BIK1/PBL1, CML41, Ca^{2+}, and potentially PDLP1/2/3, but neither strong MPK activation or ROS production. Thus, although MPK activation and ROS production are hallmarks of PTI (DeFalco and Zipfel 2021), dsRNA likely activates a specific pathway to regulate PD. Our observation that MP suppresses PD callose deposition when induced by poly(I:C) but not when induced by flg22 (Fig. 7, K and L) is consistent with this hypothesis. Importantly, we found that poly(I:C) treatment triggers BIK1 phosphorylation and that the level of poly(I:C)-induced BIK1 phosphorylation depends on SERK1, thus potentially suggesting the existence of dsRNA-perceiving SERK1-containing receptor complex that signals to BIK1. Alternatively, dsRNA may induce yet nonidentified signaling molecules that are signaled through SERK1 and BIK1. The PD-localized CML41 protein was previously shown to participate in flg22-triggered, but not chitin-triggered PD callose deposition (Xu et al. 2017). Thus, although differing in upstream components, dsRNA-induced signaling may target PD-associated regulatory components also regulated by flg22. The absence of poly(I:C)-induced ROS signaling could reflect this specific elicitor type or a specific location of perception. Bacterial and fungal PAMPs are released in the apoplast and perceived by PRRs at the PM, while viral dsRNA formation and perception may occur at intracellular membranes where viruses replicate. RIG-I-like receptors (RLRs) including RIG-I, MDA5 and LGP2 detect the presence of dsRNA in animals (Tan et al. 2018) and provide examples of dsRNA perception in the cytoplasm. Viral RNAs in animals are also recognized by Toll-like receptors in endosomes following internalization by dendritic cells and macrophages. In analogy, it is known that bacterial PAMP receptor complexes in plants are internalized from the PM to endosomes and that plant receptor-complexes can signal from endosomes. Recognition of viral dsRNA may therefore occur during membrane fusion events between viral RNA-containing vesicles or membrane-associated VRCs (Niehl and Heinlein 2019). Alternatively, the cytoplasmic dsRNA may be exported into the apoplast to be sensed by the PM-resident PRRs (Fig. 10A).

A precedent for the transport of functional RNA molecules across plant membranes is provided by cross-kingdom RNAi (Huang et al. 2019). For example, dsRNAs sprayed onto plants were shown to inhibit fungal growth in tissues distant from the sprayed tissues by inducing RNAi against essential fungal genes thus suggesting that applied dsRNAs are taken up by plants and that either dsRNAs or derived small RNAs processed within cells are able to reach the fungus in distant tissues (Koch et al. 2016). Moreover, emerging evidence suggest the presence of viral particles, viral proteins, and viral

RNA in the apoplast of infected plants (Wan et al 2015; Wan and Laliberté 2015; Movahed et al. 2019; Hu et al. 2021). Consistently, extracellular vesicles that are secreted from plants cells and are present in apoplastic fluid contain various RNA species, including viral RNA (Cai et al. 2018, 2021; Ruf et al. 2022). Poly(I:C) used in this study may mimic these potential pathways by entering plant cells upon treatment (Fig. 9), which is consistent with dsRNA perception in the cytoplasm, or by its sensing in the apoplast, either upon secretion or before cell entry (Fig. 10, A and B).

Plant viruses like TMV and ORMV undergo early replication stages at punctate, cortical microtubule-associated ER sites in close vicinity of the PM (potentially ER:PM contact sites (Pitzalis and Heinlein 2017; Huang and Heinlein 2022)), which may facilitate dsRNA perception through membrane fusion events or dsRNA secretion from the VRCs and activation of PM-localized signaling proteins in the apoplast (Niehl and Heinlein 2019). DRB2 and other double-stranded RNA binding proteins (DRBs) recently shown to accumulate in VRCs and to play a role in virus accumulation (Incarbone et al. 2021) or virus-induced necrosis (Fátyol et al. 2020) could have an important function in dsRNA sensing. Importantly, dsRNA-induced innate immunity is unaffected by mutations in dsRNA binding DICER-LIKE (DCL) proteins, which excludes these proteins as the dsRNA receptors for PTI and also shows that dsRNA silencing and dsRNA-induced innate immunity require different protein machinery (Niehl et al. 2016). The two different antiviral defense responses are also spatially separated. Inactivating the TMV VSR causes virus silencing but has no effect on virus movement and causes potent antiviral silencing only in cells behind the front engaged in virus replication for the production of virus progeny (Kubota et al. 2003; Vogler et al. 2007). Thus, we propose a model whereby a virus requires MP as viral virulence effector in cells at the infection front to suppress dsRNA-triggered PTI to support virus movement, whereas a VSR is required as virulence effector in cells behind the front to suppress dsRNA-induced silencing for producing viral progeny (Fig. 10C).

It will be interesting to dissect how the SERK1-BIK1/PBL1 module signals to CML41 and PDLP1/2/3 to regulate PD callose deposition. It is possible that BIK1/PBL1 may interact with and phosphorylate directly PDLPs in mediating callose deposition at the PD. It has been shown that the PM-tethered BIK1 regulates PAMP-triggered calcium signals by directly phosphorylating cyclic nucleotide-gated channel 2 and 4 (CNGC2/4), whose activities can be regulated by CAM7 (Tian et al. 2019). Additionally, BIK1 also phosphorylates a calcium-permeable channel, HYPEROSMOLALITY-INDUCED [Ca^{2+}] INCREASE 1.3 (OSCA1.3) in regulating stomatal immunity (Thor et al. 2020). Our observation that the calcium-chelating EGTA inhibits dsRNA-induced PD callose deposition supports the involvement of the calcium binding protein CML41 and calcium signaling in PD regulation. Therefore, it will be interesting to determine if any calcium channels directly regulated by BIK1/PBL1 and modulated by CML41 may be involved in mediating calcium signaling in plant antiviral immunity. This will help to delineate a genetic and biochemical signaling pathway linking SERKs-RLCKs-calcium channels/CML41-PDLP1/2/3 to calcium signals in regulating PD and plant antiviral immunity. It has been shown that SERK3/BAK1 plays a role in antiviral defense (Kørner et al. 2013) but the molecular mechanism remains to be explored. While poly(I:C)-induced ethylene production was not affected in *serk3/bak1* mutants (Niehl et al. 2016), it remains to be tested if SERK3/BAK1 or also SERK2 or SERK4 could play a role in dsRNA sensing leading to PD callose deposition, thus potentially explaining cases of *serk1*-independent dsRNA-induced gene activation (Fig. 2A) as well as the residual poly(I:C)-induced activation of PD callose deposition in *serk1* mutants (Fig. 3E).

In conclusion, we found that as a plant defense mechanism, dsRNA-induced antiviral PTI targets PD for callose deposition through some shared typical PTI signaling components with distinct features. To counteract this and launch efficient infections, viral MPs could effectively suppress dsRNA-induced callose deposition at PD, thus leading to a revised view of the plant–virus interaction arms-race. This study calls upon the identification of the PTI dsRNA receptor, the mechanisms of SERK1-BIK1-calcium channels/CML41-PDLP1/2/3 signaling and PTI suppression by MP, and how dsRNA-induced PTI and RNA silencing are controlled during the spread of infection, all of which present exciting challenges for additional studies.

Materials and methods

Plant materials and growth conditions

N. benthamiana and *A. thaliana* plants were grown from seeds in soil (LAT-Terra Standard Topferde Struktur 1b, Hawita, Vechta, Germany) complemented with 2,5 g/L fertilizer (Osmocote 12-7-19 +TE). *N. benthamiana* were kept under 16 h/8 h light/dark periods at +22°C/+18°C in a greenhouse equipped with Philips SON-T 400 W HPS Lamps (200 to 250 μmol/m^2/s). *A. thaliana* plants were kept under 12 h/12 h light/dark periods at +21°C/+18°C in a growth chamber equipped with Philips 20W 840 T8 LED lights (160 to 175 μmol/m^2/s). MP:RFP-transgenic *N. benthamiana* plants were produced by leaf disk transformation (Horsch et al. 1985) using binary plasmid pK7-MP:RFP (Boutant et al. 2010). The plasmid was constructed by inserting the MP coding sequence of TMV into pK7RWG2 using Gateway procedures. *N. benthamiana* plants expressing GFP-fused Flock house virus B2 protein have been described previously (Monsion et al. 2018) and were provided by Christophe Ritzenthaler (IBMP, CNRS, Strasbourg, France).

The Arabidopsis mutants used in this study have been described previously and homozygous seeds were kind provided from different research laboratories. Seeds of the *bik1 pbl1* double mutant (SALK_005291 SAIL_1236_D07) (Zhang et al. 2010) were provided by Cyril Zipfel (University of Zürich, Switzerland). *mpk3-1* (SALK_151594) and *mpk6-2* (SALK_073907) lines were given by Kenichi

Tsuda (Max Planck Institute for Plant Breeding research, Cologne, Germany) and, together with seeds of the *mpk3amiRmpk6* (Li et al. 2014) and *serk1-1* (SALK_044330) (Meng et al. 2015b) mutants, also by the author Libo Shan. Seeds of *CML41* overexpressing and silenced lines (*CML41-OEX-2*, *CML41-OEX-12*, *CML41-amiRNA-1* and *CML41-amiRNA-4*) (Xu et al. 2017) were a gift of Matthew Gilliham (University of Adelaide, Australia). Arabidopsis lines transgenic for PD markers mCherry-BDCB1 (Simpson et al. 2009; Benitez-Alfonso et al. 2013) or PdBG2-citrine (Benitez-Alfonso et al. 2013) were provided by Yoselin Benitez-Alfonso (University of Leeds, UK).

Virus inoculation

cDNA constructs for TMV-MP:RFP (Ashby et al. 2006), TMV-GFP (Heinlein et al. 1995), and TMVΔM-GFP (Vogler et al. 2008) have been described previously. *N. benthamiana* plants were mechanically inoculated in the presence of an abrasive (Celite545) with infectious RNA in vitro-transcribed from these constructs. A TMV replicon (TMV-ΔMP-ΔCP-GFP) cloned in a binary vector for agroinfiltration and used for testing virus replication and movement trans-complementation has been described (Borniego et al. 2016). Arabidopsis plants were inoculated with purified ORMV virions (Niehl et al. 2012).

Analysis of virus infection in the presence of elicitors

To test the effect of elicitors on TMV-GFP infection in *N. benthamiana*, plants were inoculated with 200 μL inoculum containing 20 μL of infectious viral RNA transcription mix and 0.5 μg/μL (equals ~1 μM) poly(I:C) (Sigma-Aldrich, USA), or 1 μM flg22 (EZBiolabs, USA or Proteogenix, France), or water. Infection sites on the inoculated leaves were imaged using a hand-held camera and UV lamp (BLAK RAY B-100AP; UVP Inc., Upland, California) in the presence of a ruler for size normalization. The areas of infection sites in each leaf were measured with Image J software upon selection of infection site as regions of interest using fluorescence thresholding and the wand tracing tool, and by setting the scale according to the ruler. For testing the effect of poly(I:C) on viral replication, *N. benthamiana* leaves were agro-inoculated with a MP-deficient, cell-autonomous TMV replicon (TMVΔMP-ΔCP-GFP) (Borniego et al. 2016). After 1 d, the fluorescent leaf patches were gently rubbed with 200 μL of 0.5 μg/μL poly(I:C) in the presence of celite. At 1, 3, and 5 d after this treatment, the GFP-expressing leaf patches were analyzed for viral RNA accumulation by quantitative Taqman reverse transcription quantitative PCR (RT-qPCR) using previously described methods (Mansilla et al. 2009; Niehl et al. 2016).

To test the effect of elicitors on ORMV infection in Arabidopsis, 4 μL of elicitor solution (10 μg/mL poly(I:C) or 10 μM flg22) or 4 μL PBS were placed on rosette leaves of 3-wk-old Arabidopsis wildtype or mutant Col-0 plants. A volume of 2.5 μL of a 20 ng/μL solution of purified ORMV virions was placed on the same leaves. Subsequently, the leaves were gently rubbed in the presence of celite as abrasive. Immediately after treatment, remaining elicitors, buffers and virions were washed off the leaf surface. Symptoms were analyzed at 28 dpi. At the same time young, systemic leaves were sampled for analysis of virus accumulation by quantitative Taqman RT-qPCR using previously described methods (Mansilla et al. 2009; Niehl et al. 2016).

Analysis of differential gene expression by RT-qPCR

N. benthamiana or Arabidopsis Col-0 leaf disks were excised with a cork borer and incubated overnight in 12-well plates containing 600 μL deionized, ultra-pure water. The leaf disks were washed several times with water and then incubated with elicitor (1 μM flg22, 0.5 μg/μL poly(I:C), or water as control) for 3 h. After washing the disks with deionized, ultrapure water 3 times, samples were ground to a fine powder in liquid nitrogen and total RNA was extracted by TRIzol reagent according to the protocol of the manufacturer. Two micrograms of RNA were reverse transcribed using a reverse transcription kit (GoScript Reverse Transcription System, Promega). The abundance of specific transcript was measured by probing 1 μL cDNA by quantitative real-time PCR in a total volume of 10 μL containing 5 μL SYBR-green master mix (Roche), 0.5 μM forward and reverse primer and water. qPCR was performed in a Lightcycler480 (Roche) using a temperature regime consisting of 5 min at 95°C followed by 45 cycles at 95°C for 10 s, 60°C for 15 s, and 72°C for 15 s, and ending with a cycle of 95°C for 5 s, 55°C for 60 s, 95°C for continuous time until final cooling to 40°C for 30 s. The threshold cycle (CT) values were normalized to CT-values obtained for reference genes *ACTIN2* and *UBIQUITIN10* (Czechowski et al. 2005), providing ΔCT values. These were used to calculate the $2^{-\Delta CT}$ values representing relative expression levels, the mean values and SE. Each mean value represents the analysis of 3 independent replicate samples (individual plants treated the same way and harvested at the same time), each measured by 3 technical replicates. Primers are listed in Supplemental Table S1.

Transient expression of proteins by agroinfiltration

Binary plasmids for transient expression of RFP and of TMV-derived MP:RFP, MP:GFP, MP^{C55}:GFP, and MP^{P81S}:GFP as well as of MP^{ORMV}:RFP and MP^{TVCV}:RFP were created by Gateway cloning as has been described previously (Brandner et al. 2008; Sambade et al. 2008; Boutant et al. 2010).

For transient expression of the fluorescent fusion proteins, cultures of *A. tumefaciens* bacteria (strain GV3101) carrying these plasmids were harvested by centrifugation, resuspended in infiltration medium (10 mM MES, 10 mM $MgCl_2$, 200 μM acetosyringone; pH 5.5) to a final optical density at 600 nm (OD_{600}) of 0.1 (unless stated differently), and infiltrated into the abaxial side of the leaf using a syringe without a needle. Leaves were observed by confocal microscopy at 48 h after agroinfiltration.

For GFP mobility assays, we used Agrobacteria that were cotransformed with binary vectors for expression of GFP together with the cell-autonomous nuclear protein NLS:RFP

(pB7-NLS:M2CP:RFP; this vector was created by recombining pZeo-NLS:MS2CP (Sambade et al. 2008) with expression vector pH7RWG2). The 2 binary vectors carry different resistance genes and their presence in the same agrobacteria was maintained by appropriate antibiotic coselection. Before infiltration, the diluted culture ($OD_{600} = 0.1$) was further diluted 1:1,000 or 1:10,000 to ensure expression of both proteins in only few cells of the leaf. Twenty-four hours after infiltration, the agroinfiltrated leaves were detached and analyzed by confocal microscopy, revealing about 10 to 15 single cell transformation events with both markers. The levels of cytoplasmic GFP and nuclear NLS:RFP differed between the transformed cells but cells expressing only GFP or only NLS:GFP were not observed, which excludes the occurrence of transformation events in which only one of the T-DNAs was transferred. Subsequently, leaf disks with the single cell transformation events were excised and incubated in 0.5 μg/μL poly(I:C) or water for 48 h. Finally, each of the transformation events was evaluated for GFP movement by confocal microscopy by counting the radial cell layers into which GFP has moved away from the infiltrated cell (marked by red fluorescent nucleus). The statistical significance between nonparametric GFP movement data obtained for water-treated and poly(I:C)-treated tissues was determined by a Mann–Whitney test. As this test provides a *P*-value for the difference in data distributions rather than the means, the statistical *P*-value for the difference in mean values (p^{bs}) was determined by a bootstrap function in R (Johnston and Faulkner 2021) using 5,000 resampling steps. For movement trans-complementation assays, *N. benthamiana* leaves were infiltrated with *Agrobacterium* cultures ($OD_{600\ nm} = 0.3$) for the expression of either MP^{TMV}:mRFP MP^{ORMV}:mRFP, MP^{TVCV}:mRFP or of free mRFP together with a highly diluted *Agrobacterium* culture for infection of single cells with TMVΔMPΔCP-GFP ($OD_{600\ nm} = 1 \times 10^{-5}$). Fluorescent infection sites indicating complementation of the MP-deficient virus were imaged with a Nikon D80 camera at 5 dpi under UV illumination. For the movement trans-complementation assay with MP:RFP-transgenic *N. benthamiana* plants, leaves were inoculated with infectious RNA in vitro-transcribed from pTMVΔM-GFP (Vogler et al. 2008) and infection sites were observed at 7 dpi.

Callose staining

Leaf disks were excised with a cork borer and placed into wells of 12-well culture plates containing 1 mL water and incubated overnight under conditions at which the plants were raised. The leaf disks were washed several times with water before use. For callose staining, individual leaf disks were placed on microscope slides and covered with a coverslip fixed with tape. If not otherwise stated, 200 μL of a 1% aniline blue solution (in 50 mM potassium phosphate buffer, pH 8.0) containing either 0.5 μg/μL poly(I:C), 50 ng/μL $dsRNA^{phi6}$ or 1 μm flg22 were soaked into the space between the glass slide and coverslip. The glass slide with the sample was evacuated for 1 to 2 min (< 0.8 Pa) in a vacuum desiccator followed by slow release of the pressure. Aniline blue fluorescence was imaged 30 min after dsRNA or control treatment using a Zeiss LSM 780 confocal laser scanning microscope with ZEN 2.3 software (Carl Zeiss, Jean, Germany) and using a 405 nm diode laser for excitation and filtering the emission at 475 to 525 nm. Eight-bit images acquired with a 40× 1.3 N.A. Plan Neofluar objective with oil immersion were analyzed with ImageJ software (http://rsbweb.nih. gov/ij/) using the plug-in *calloseQuant*, which after setting few parameters localizes fluorescent callose spots and quantifies callose fluorescence intensity of each spot automatically (Huang et al. 2022). This plugin is available at https://raw.githubusercontent.com/mutterer/callose/main/calloseQuant_.ijm. Callose spots were measured in 1 to 5 images taken from each leaf disk. If not otherwise mentioned, 3 leaf disks from 3 different plants were evaluated for each genotype or condition. To control for normal poly(I:C) treatment and callose staining conditions, samples of Arabidopsis mutants were always analyzed in parallel to samples from the Col-0 wild-type. Similarly, samples from agroinfiltrated MP:GFP/RFP-expressing *N. benthamiana* leaves were compared with samples from agroinfiltrated GFP/RFP-expressing control leaves. Regions of interest (ROIs) selected by *calloseQuant* were verified visually one by one before measurement. ROIs that were not overlapping with the cell wall or did not contain clear signal above the background were deleted. Moreover, individual fluorescence intensities that occurred as outliers from the general distribution of fluorescence intensities (<1%) in the sample were excluded from analysis. For any given experiment, selected ROI size radius was determined according to the size of the largest PD-associated signal present in any image and this ROI size was kept constant for all the images. Background pixels within ROIs associated with low signal in the center of the ROI may have contributed to the baseline callose signal in control conditions thus potentially reducing the fold-change of signal upon treatment. The mean fluorescence intensities obtained for the specific genotypes or treatment conditions are shown in column diagrams. *P*-values for the statistical difference between the mean value data were determined by an ordinary *t*-test or by 1-way ANOVA followed by Sidak's pairwise comparisons (e.g. treatment versus control). The statistical tests were performed with GraphPad Prism 8 software.

Analysis of MPK activation

Leaf disks from 4-wk-old *A. thaliana* or *N. benthamiana* plants were elicited with 1 μM flg22 or 0.5 μg/μL (equals ~1 μM) poly(I:C). As a control, leaf disks were treated with water or treated with PBS. Elicitor and control treatment was performed by addition of the elicitor or the controls to leaf disks acclimated overnight in ultrapure water. After addition of the elicitor, leaf disks were vacuum infiltrated for 10 min. Samples were taken after an additional 20 min of incubation. MPK phosphorylation was determined using protein extracts obtained from elicitor or control-treated leaf disks using immunoblots probed with 1:2000-diluted antibodies against phosphor-p44/42 ERK (Cell Signaling Technology, Beverly, MA, USA; Ozyme #S4370S) and 1:10000-diluted horseradish peroxidase (HRP)-labelled

secondary antibodies (Thermo Fisher Scientific, #31460) for luminescence detection (SuperSignal West Femto Maximum Sensitivity Substrate, Thermo Fisher Scientific).

Analysis of ROS production

Leaf disks excised from 4-wk-old *A. thaliana* or *N. benthamiana* plants were incubated overnight in 96-well plates with 600 μL of deionized, ultra-pure water. The next day deionized, ultra-pure water was replaced with 100 μL reaction solution containing 50 μM luminol and 10 μg/mL horseradish peroxidase (Sigma, USA) together with or without 1 μM flg22 or 0.5 μg/μL poly(I:C). Luminescence was determined with a luminometer (BMG LABTECH, FLUOstarOmega) at 1.5 min intervals for a period of 40 min. Mean values obtained for 10 leaf disks per treatment were expressed as mean relative light units (RLUs).

Seedling growth inhibition assay

Seeds were surface-sterilized and grown vertically at 22 °C under 12 h/12 h light/dark periods in square petri-dishes on half-strength MS basal medium (pH 5.8) containing 0.5 g/L MES and 0.8% agar. Seven-day-old seedlings were transferred into liquid half-strength MS medium with or without 500 ng/μL (equals ~1 μM) poly(I:C) or 1 μM flg22. The effect of treatment on seedling growth was documented on photographs 12 d after treatment and measured with a ruler.

Protoplast transient expression and BIK1 mobility shift assays

Arabidopsis protoplasts (about 40,000 cells) isolated from wild-type Col-0 or *serk1-1* were transfected with HA-epitope-tagged BIK1 (pHBT-35S:BIK1-HA) or cotransfected with pHBT-35S:BIK1-HA and pHBT-35S:SERK1-FLAG. Protoplast isolation and the transient expression assay were done as described previously (He et al. 2007). Also the BIK1 and SERK1 constructs have already been described (Lu et al. 2010; Meng et al. 2015a). The transfected protoplasts were incubated at room temperature overnight. After stimulation with flg22 (1 μM) or poly(I:C) (0.5 μg/uL) for 20 min, the protoplasts were collected by centrifugation and lysed by vortexing in 100 μL co-IP buffer (150 mM NaCl, 50 mM Tris-HCl, pH7.5, 5 mM EDTA, 0.5% Triton, 1 × protease inhibitor cocktail. Before use, 2.5 μL 0.4 M DTT, 2 μL 1 M NaF and 2 μL 1 M Na_3VO_3 were added per 1 ml IP buffer). A final concentration of 1 μM K-252a inhibitor (Sigma-Aldrich, 05288) was added 1 h before poly(I:C) (0.5 μg/uL) treatment. Lysed protoplasts were treated with calf intestinal phosphatase (CIP) (New England Biolabs, #M0290) for 60 min at 37 °C (1 unit per μg of total protein). BIK1 was detected by immunoblots using 1:2000-diluted HA-HRP antibody (Invitrogen, #26183-HRP) and its phosphorylation was quantified by calculating the ratio between the intensity of the shifted upper band of phosphorylated BIK1 (pBIK1) and the sum of the intensities of both shifted and nonshifted bands (pBIK1 + BIK1) (no treatment set to 0.0). The BIK1 mobility shift assays have been described previously (Lu et al. 2010; Ma et al. 2020). SERK1-FLAG was detected in immunoblot assays using 1:2000-diluted monoclonal anti-FLAG (Sigma-Aldrich, #F1804).

Imaging

Microscopical imaging was performed with a Zeiss LSM 780 confocal laser scanning microscope equipped with ZEN 2.3 software (Carl Zeiss, Jean, Germany). Excitation/emission wavelengths were 405 nm/475 to 525 nm for aniline blue, 488 nm/500 to 525 nm for GFP, and 561 nm/560–610 nm for RFP.

Statistical analysis

Statistical data are provided in Supplemental Data Set S1.

Accession numbers

Sequence data for Arabidopsis genes mentioned in this article can be found at The Arabidopsis Information Resource (https://www.arabidopsis.org/) under accession numbers: *PdBG2* (AT2G01630), *PDCB1* (AT5G61130), *PDLP1* (AT5G43980), *PDLP2* (AT1G04520), *PDLP3* (AT2G33330), *PDLP5* (AT1G70690), *BIK1* (AT2G39660), *PBL1* (AT3G55450), *SERK1* (AT1G71830), *MPK3* (AT3G45640), *MPK6* (AT2G43790), *CML41* (AT3G50770), *PAD4* (AT3G52430), *PAL1* (AT2G37040), *PDF1.2* (AT5G44420), *FRK1* (AT2G19190), *PR2* (AT3G57260), and *PR5* (AT1G75040). Sequence data for *Nicotiana benthamiana* genes mentioned in this article can be found at GenBank (https://www.ncbi.nlm.nih.gov/nuccore/) under accession numbers: *BRI1* (EF471738.1), *BIK1* (KM249875.1), *PR2* (M60460.1), *RBOHB* (LC156098.1), and *EDS1* (AF479625.1).

Acknowledgments

We acknowledge funding from the Agence National de la Recherche (Plant-KBBE2012/ANR-13-KBBE-0005-01, ERA-NET SusCrop2/ANR-21-SUSC-0003-01; ANR-PRC/ANR-21-CE20-0020-01) and the China Scholarship Council (No. 201706300035, PhD fellowship for C.H.) to M.H. and funding from the NIH (R35GM144275), NSF (IOS-2049642), and the Robert A. Welch Foundation (A-2122-20220331) to L.S. We thank Cyril Zipfel, Christine Faulkner, Matthew Gilliham, Kenichi Tsuda, Christophe Ritzenthaler, and Yoselin Benitez-Alfonso for providing seeds of Arabidopsis mutants and transgenic lines. We also thank Minna Poranen (University of Helsinki, Finland) for providing Phi6 dsRNA.

Author contributions

Conceptualization: M.H.; methodology: C.H., J.M., E.B., Y.Y., M.R., A.R.S., L.E.-G., L.S., and M.H.; investigation: C.H., A.R.S., L.E.-G., Y.Y., M.R., and M.H.; visualization: C.H., A.R.S., L.E.-G., Y.Y., L.S., and M.H.; funding acquisition: L.S. and M.H.; project administration: M.H.; supervision: L.S. and M.H.; writing—original draft: M.H.; writing—review and editing: C.H., A.R.S., L.E.-G., J.M., L.S., and M.H.

Supplemental data

The following materials are available in the online version of this article.

Supplemental Figure S1. Poly(I:C) treatment inhibits the cell-to-cell spread of TMV-GFP infection in *N. benthamiana* leaves.

Supplemental Table S1. Primers used for RT-qPCR.

Supplemental Data Set S1. Statistical analyses.

Conflict of interest statement. The authors declare to have no conflicts of interest.

Data availability

All data are available in the main text or the Supplemental materials.

References

Alexopoulou L, Holt AC, Medzhitov R, Flavell RA. Recognition of double-stranded RNA and activation of NF-kappaB by toll-like receptor 3. Nature. 2001:**413**(6857):732–738. https://doi.org/10.1038/35099560

Amari K, Boutant E, Hofmann C, Schmitt-Keichinger C, Fernandez-Calvino L, Didier P, Lerich A, Mutterer J, Thomas CL, Heinlein M, et al. A family of plasmodesmal proteins with receptor-like properties for plant viral movement proteins. PLoS Pathog. 2010:**6**(9):e1001119. https://doi.org/10.1371/journal.ppat.1001119

Ashby J, Boutant E, Seemanpillai M, Groner A, Sambade A, Ritzenthaler C, Heinlein M. *Tobacco mosaic virus* movement protein functions as a structural microtubule-associated protein. J Virol. 2006:**80**(17):8329–8344. https://doi.org/10.1128/JVI.00540-06

Beffa RS, Hofer RM, Thomas M, Meins F. Decreased susceptibility to viral disease of [beta]-1,3-glucanase-deficient plants generated by antisense transformation. Plant Cell. 1996:**8**(6):1001–1011. https://doi.org/10.2307/3870211

Benitez-Alfonso Y, Faulkner C, Pendle A, Miyashima S, Helariutta Y, Maule A. Symplastic intercellular connectivity regulates lateral root patterning. Dev Cell. 2013:**26**(2):136–147. https://doi.org/10.1016/j.devcel.2013.06.010

Borniego MB, Karlin D, Pena EJ, Robles Luna G, Garcia ML. Bioinformatic and mutational analysis of ophiovirus movement proteins, belonging to the 30K superfamily. Virology. 2016:**498**:172–180. https://doi.org/10.1016/j.virol.2016.08.027

Boutant E, Didier P, Niehl A, Mély Y, Ritzenthaler C, Heinlein M. Fluorescent protein recruitment assay for demonstration and analysis of in vivo protein interactions in plant cells and its application to *Tobacco mosaic virus* movement protein. Plant J. 2010:**62**(1):171–177. https://doi.org/10.1111/j.1365-313X.2010.04126.x

Boyko V, Ashby JA, Suslova E, Ferralli J, Sterthaus O, Deom CM, Heinlein M. Intramolecular complementing mutations in *tobacco mosaic virus* movement protein confirm a role for microtubule association in viral RNA transport. J Virol. 2002:**76**(8):3974–3980. https://doi.org/10.1128/JVI.76.8.3974-3980.2002

Boyko V, van der Laak J, Ferralli J, Suslova E, Kwon M-O, Heinlein M. Cellular targets of functional and dysfunctional mutants of *Tobacco mosaic virus* movement protein fused to GFP. J Virol. 2000:**74**(23):11339–11346. https://doi.org/10.1128/JVI.74.23.11339-11346.2000

Brandner K, Sambade A, Boutant E, Didier P, Mély Y, Ritzenthaler C, Heinlein M. *Tobacco mosaic virus* movement protein interacts with green fluorescent protein-tagged microtubule end-binding protein 1. Plant Physiol. 2008:**147**(2):611–623. https://doi.org/10.1104/pp.108.117481

Brault ML, Petit JD, Immel F, Nicolas WJ, Glavier M, Brocard L, Gaston A, Fouche M, Hawkins TJ, Crowet JM, et al. Multiple C2 domains and transmembrane region proteins (MCTPs) tether membranes at plasmodesmata. EMBO Rep. 2019:**20**(8):e47182. https://doi.org/10.15252/embr.201847182

Bucher GL, Tarina C, Heinlein M, Di Serio F, Meins F, Iglesias VA. Local expression of enzymatically active class 1 beta-1,3-glucanase enhances symptoms of TMV infection in tobacco. Plant J. 2001:**28**(3):361–369. https://doi.org/10.1046/j.1365-313X.2001.01181.x

Cai Q, He B, Wang S, Fletcher S, Niu D, Mitter N, Birch PRJ, Jin H. Message in a bubble: shuttling small RNAs and proteins between cells and interacting organisms using extracellular vesicles. Annu Rev Plant Biol. 2021:**72**(1):497–524. https://doi.org/10.1146/annurev-arplant-081720-010616

Cai Q, Qiao L, Wang M, He B, Lin F-M, Palmquist J, Huang S-D, Jin H. Plants send small RNAs in extracellular vesicles to fungal pathogen to silence virulence genes. Science. 2018:**360**(6393):1126–1129. https://doi.org/10.1126/science.aar4142

Caillaud MC, Wirthmueller L, Sklenar J, Findlay K, Piquerez SJM, Jones AM, Robatzek S, Jones JD, Faulkner C. The plasmodesmal protein PDLP1 localises to haustoria-associated membranes during downy mildew infection and regulates callose deposition. PLoS Pathog. 2014:**10**(11):e1004496. https://doi.org/10.1371/journal.ppat.1004496

Castro B, Citterico M, Kimura S, Stevens DM, Wrzaczek M, Coaker G. Stress-induced reactive oxygen species compartmentalization, perception and signalling. Nat Plants. 2021:**7**(4):403–412. https://doi.org/10.1038/s41477-021-00887-0

Chen MH, Shen J, Hind G, Handa AK, Citovsky V. Interaction between the tobacco mosaic virus movement protein and host cell pectin methylesterases is required for viral cell-to-cell movement. EMBO J. 2000:**19**(5):913–920. https://doi.org/10.1093/emboj/19.5.913

Cheval C, Samwald S, Johnston MG, de Keijzer J, Breakspear A, Liu X, Bellandi A, Kadota Y, Zipfel C, Faulkner C. Chitin perception in plasmodesmata characterizes submembrane immune-signaling specificity in plants. Proc Natl Acad Sci U S A. 2020:**117**(17):9621–9629. https://doi.org/10.1073/pnas.1907799117

Christensen N, Tilsner J, Bell K, Hammann P, Parton R, Lacomme C, Oparka K. The 5′ Cap of *Tobacco mosaic virus* (TMV) is required for virion attachment to the actin/endoplasmic reticulum network during early infection. Traffic. 2009:**10**(5):536–551. https://doi.org/10.1111/j.1600-0854.2009.00889.x

Citovsky V. *Tobacco mosaic virus*: a pioneer of cell-to-cell movement. Philos Trans R Soc Lond B Biol Sci. 1999:**354**(1383):637–643. https://doi.org/10.1098/rstb.1999.0415

Citovsky V, Knorr D, Schuster G, Zambryski P. The P30 movement protein of *Tobacco mosaic virus* is a single-strand nucleic acid binding protein. Cell. 1990:**60**(4):637–647. https://doi.org/10.1016/0092-8674(90)90667-4

Csorba T, Kontra L, Burgyan J. Viral silencing suppressors: tools forged to fine-tune host-pathogen coexistence. Virology. 2015:**479–480**:85–103. https://doi.org/10.1016/j.virol.2015.02.028

Czechowski T, Stitt M, Altmann T, Udvardi MK, Scheible WR. Genome-wide identification and testing of superior reference genes for transcript normalization in Arabidopsis. Plant Physiol. 2005:**139**(1):5–17. https://doi.org/10.1104/pp.105.063743

DeFalco TA, Zipfel C. Molecular mechanisms of early plant pattern-triggered immune signaling. Mol Cell. 2021:**81**(17):3449–3467. https://doi.org/10.1016/j.molcel.2021.07.029

De Storme N, Geelen D. Callose homeostasis at plasmodesmata: molecular regulators and developmental relevance. Front Plant Sci. 2014:**5**:138. https://doi.org/10.3389/fpls.2014.00138

Ding B, Haudenshield JS, Hull RJ, Wolf S, Beachy RN, Lucas WJ. Secondary plasmodesmata are specific sites of localization of the *Tobacco mosaic virus* movement protein in transgenic tobacco

plants. Plant Cell. 1992:**4**(8):915–928. https://doi.org/10.1105/tpc.4.8.915

Dolja VV, Krupovic M, Koonin EV. Deep roots and splendid boughs of the global plant virome. Annu Rev Phytopathol. 2020:**58**(1):23–53. https://doi.org/10.1146/annurev-phyto-030320-041346

Fátyol K, Fekete KA, Ludman M. Double-stranded-RNA-binding protein 2 participates in antiviral defense. J Virol. 2020:**94**(11):e00017-20. https://doi.org/10.1128/JVI.00017-20

Faulkner C, Petutschnig E, Benitez-Alfonso Y, Beck M, Robatzek S, Lipka V, Maule AJ. LYM2-dependent Chitin perception limits molecular flux via plasmodesmata. Proc Natl Acad Sci U S A. 2013:**110**(22):9166–9170. https://doi.org/10.1073/pnas.1203458110

Guenoune-Gelbart D, Elbaum M, Sagi G, Levy A, Epel BL. *Tobacco mosaic virus* (TMV) replicase and movement protein function synergistically in facilitating TMV spread by lateral diffusion in the plasmodesmal desmotubule of *Nicotiana benthamiana*. Mol Plant Microbe Interact. 2008:**21**(3):335–345. https://doi.org/10.1094/MPMI-21-3-0335

Guseman JM, Lee JS, Bogenschutz NL, Peterson KM, Virata RE, Xie B, Kanaoka MM, Hong Z, Torii KU. Dysregulation of cell-to-cell connectivity and stomatal patterning by loss-of-function mutation in Arabidopsis *chorus* (glucan synthase-like 8). Development. 2010:**137**(10):1731–1741. https://doi.org/10.1242/dev.049197

He P, Shan L, Sheen J. The use of protoplasts to study innate immune responses. Methods Mol Biol. 2007:**354**:1–9. https://doi.org/10.1385/1-59259-966-4:1

Heinlein M. Plant virus replication and movement. Virology. 2015:**479-480**:657–671. https://doi.org/10.1016/j.virol.2015.01.025

Heinlein M, Epel BL, Padgett HS, Beachy RN. Interaction of tobamovirus movement proteins with the plant cytoskeleton. Science. 1995:**270**(5244):1983–1985. https://doi.org/10.1126/science.270.5244.1983

Heinlein M, Wood MR, Thiel T, Beachy RN. Targeting and modification of prokaryotic cell-cell junctions by *Tobacco mosaic virus* cell-to-cell movement protein. Plant J. 1998:**14**(3):345–351. https://doi.org/10.1046/j.1365-313X.1998.00118.x

Holdaway-Clarke TL, Walker NA, Hepler PK, Overall RL. Physiological elevations in cytoplasmic free calcium by cold or ion injection result in transient closure of higher plant plasmodesmata. Planta. 2000:**210**(2):329–335. https://doi.org/10.1007/PL00008141

Horsch AB, Fry JE, Hoffmann NL, Wallroth M, Eichholtz D, Rogers SG, Fraley RT. A simple and general method for transferring genes into plants. Science. 1985:**227**(4691):1229–1231. https://doi.org/10.1126/science.227.4691.1229

Hu S, Yin Y, Chen B, Lin Q, Tian Y, Song X, Peng J, Zheng H, Rao S, Wu G, et al. Identification of viral particles in the apoplast of *Nicotiana benthamiana* leaves infected by potato virus X. Mol Plant Pathol. 2021:**22**(4):456–464. https://doi.org/10.1111/mpp.13039

Huang C, Heinlein M. Function of plasmodesmata in the interaction of plants with microbes and viruses. Methods Mol Biol. 2022:**2457**:23–54. https://doi.org/10.1007/978-1-0716-2132-5_2

Huang C, Mutterer J, Heinlein M. In vivo aniline blue staining and semi-automated quantification of callose deposition at plasmodesmata. Methods Mol Biol. 2022:**2457**:151–165. https://doi.org/10.1007/978-1-0716-2132-5_9

Huang CY, Wang H, Hu P, Hamby R, Jin H. Small RNAs – big players in plant-microbe interactions. Cell Host Microbe. 2019:**26**(2):173–182. https://doi.org/10.1016/j.chom.2019.07.021

Iglesias VA, Meins F. Movement of plant viruses is delayed in a β-1,3-glucanase-deficient mutant showing a reduced plasmodesmatal size exclusion limit and enhanced callose deposition. Plant J. 2000:**21**(2):157–166. https://doi.org/10.1046/j.1365-313x.2000.00658.x

Incarbone M, Clavel M, Monsion B, Kuhn L, Scheer H, Vantard E, Poignavent V, Dunoyer P, Genschik P, Ritzenthaler C. Immunocapture of dsRNA-bound proteins provides insight into *Tobacco rattle virus* replication complexes and reveals Arabidopsis DRB2 to be a wide-spectrum antiviral effector. Plant Cell. 2021:**33**(11):3402–3420. https://doi.org/10.1093/plcell/koab214

Ishikawa K, Tamura K, Fukao Y, Shimada T. Structural and functional relationships between plasmodesmata and plant endoplasmic reticulum-plasma membrane contact sites consisting of three synaptotagmins. New Phytol. 2020:**226**(3):798–808. https://doi.org/10.1111/nph.16391

Johnston MG, Faulkner C. A bootstrap approach is a superior statistical method for the comparison of normal data with differing variances. New Phytol. 2021:**230**(1):23–26. https://doi.org/10.1111/nph.17159

Jones RAC. Global plant virus disease pandemics and epidemics. Plants (Basel). 2021:**10**(2):233. https://doi.org/10.3390/plants10020233

Jones RAC, Naidu RA. Global dimensions of plant virus diseases: current status and future perspectives. Annu Rev Virol. 2019:**6**(1):387–409. https://doi.org/10.1146/annurev-virology-092818-015606

Kadota Y, Sklenar J, Derbyshire P, Stransfeld L, Asai S, Ntoukakis V, Jones JD, Shirasu K, Menke F, Jones A, et al. Direct regulation of the NADPH oxidase RBOHD by the PRR-associated kinase BIK1 during plant immunity. Mol Cell. 2014:**54**(1):43–55. https://doi.org/10.1016/j.molcel.2014.02.021

Koch A, Biedenkopf D, Furch A, Weber L, Rossbach O, Abdellatef E, Linicus L, Johannsmeier J, Jelonek L, Goesmann A, et al. An RNAi-based con- trol of *Fusarium graminearum* infections through spraying of long dsRNAs involves a plant passage and is controlled by the fungal silencing machinery. PLoS Pathog. 2016:**12**(10):e1005901. https://doi.org/10.1371/journal.ppat.1005901

Kørner CJ, Klauser D, Niehl A, Dominguez-Ferreras A, Chinchilla D, Boller T, Heinlein M, Hann DR. The immunity regulator BAK1 contributes to resistance against diverse RNA viruses. Mol Plant Microbe Interact. 2013:**26**(11):1271–1280. https://doi.org/10.1094/MPMI-06-13-0179-R

Kubota K, Tsuda S, Tamai A, Meshi T. *Tomato mosaic virus* replication protein suppresses virus-targeted posttranscriptional gene silencing. J Virol. 2003:**77**(20):11016–11026. https://doi.org/10.1128/JVI.77.20.11016-11026.2003

Lee JY, Lucas WJ. Phosphorylation of viral movement proteins–regulation of cell-to-cell trafficking. Trends Microbiol. 2001:**9**(1):5–8. https://doi.org/10.1016/S0966-842X(00)01901-6

Lee JY, Wang X, Cui W, Sager R, Modla S, Czymmek K, Zybaliov B, van Wijk K, Zhang C, Lu H, et al. A plasmodesmata-localized protein mediates crosstalk between cell-to-cell communication and innate immunity in Arabidopsis. Plant Cell. 2011:**23**(9):3353–3373. https://doi.org/10.1105/tpc.111.087742

Levy A, Erlanger M, Rosenthal M, Epel BL. A plasmodesmata-associated beta-1,3-glucanase in Arabidopsis. Plant J. 2007:**49**(4):669–682. https://doi.org/10.1111/j.1365-313X.2006.02986.x

Levy A, Zheng JY, Lazarowitz SG. Synaptotagmin SYTA forms ER-plasma membrane junctions that are recruited to plasmodesmata for plant virus movement. Curr Biol. 2015:**25**(15):2018–2025. https://doi.org/10.1016/j.cub.2015.06.015

Li F, Cheng C, Cui F, de Oliveira MV, Yu X, Meng X, Intorne AC, Babilonia K, Li M, Li B, et al. Modulation of RNA polymerase II phosphorylation downstream of pathogen perception orchestrates plant immunity. Cell Host Microbe. 2014:**16**(6):748–758. https://doi.org/10.1016/j.chom.2014.10.018

Lim GH, Shine MB, de Lorenzo L, Yu K, Cui W, Navarre D, Hunt AG, Lee JY, Kachroo A, Kachroo P. Plasmodesmata localizing proteins regulate transport and signaling during systemic acquired immunity in plants. Cell Host Microbe. 2016:**19**(4):541–549. https://doi.org/10.1016/j.chom.2016.03.006

Liu Z, Wu Y, Yang F, Zhang Y, Chen S, Xie Q, Tian X, Zhou JM. BIK1 Interacts with PEPRs to mediate ethylene-induced immunity. Proc Natl Acad Sci U S A. 2013:**110**(15):6205–6210. https://doi.org/10.1073/pnas.1215543110

Lopez-Gomollon S, Baulcombe DC. Roles of RNA silencing in viral and non-viral plant immunity and in the crosstalk between disease

resistance systems. Nat Rev Mol Cell Biol. 2022:**23**(10):645–662. https://doi.org/10.1038/s41580-022-00496-5

Lu D, Wu S, Gao X, Zhang Y, Shan L, He P. A receptor-like cytoplasmic kinase, BIK1, associates with a flagellin receptor complex to initiate plant innate immunity. Proc Natl Acad Sci U S A. 2010:**107**(1): 496–501. https://doi.org/10.1073/pnas.0909705107

Ma X, Claus LAN, Leslie ME, Tao K, Wu Z, Liu J, Yu X, Li B, Zhou J, Savatin DV, et al. Ligand-induced monoubiquitination of BIK1 regulates plant immunity. Nature. 2020:**581**(7807):199–203. https://doi.org/10.1038/s41586-020-2210-3

Mansilla C, Sánchez F, Padgett HS, Pogue GP, Ponz F. Chimeras between *Oilseed rape mosaic virus* and *Tobacco mosaic virus* highlight the relevant role of the tobamoviral RdRp as pathogenicity determinant in several hosts. Mol Plant Pathol. 2009:**10**(1):59–68. https://doi.org/10.1111/j.1364-3703.2008.00506.x

Meng X, Chen X, Mang H, Liu C, Yu X, Gao X, Torii KU, He P, Shan L. Differential function of Arabidopsis SERK family receptor-like kinases in stomatal patterning. Curr Biol. 2015b:**25**(18):2361–2372. https://doi.org/10.1016/j.cub.2015.07.068

Meng X, Shan L, He P. Stack heterotrimeric G proteins and MAPK cascades on a RACK. Mol Plant. 2015a:**8**(12):1691–1693. https://doi.org/10.1016/j.molp.2015.11.005

Mittler R. ROS Are good. Trends Plant Sci. 2017:**22**(1):11–19. https://doi.org/10.1016/j.tplants.2016.08.002

Monsion B, Incarbone M, Hleibieh K, Poignavent V, Ghannam A, Dunoyer P, Daeffler L, Tilsner J, Ritzenthaler C. Efficient detection of long dsRNA i*n vitro* and *in vivo* using the dsRNA binding domain from FHV B2 protein. Front Plant Sci. 2018:**9**:70. https://doi.org/10.3389/fpls.2018.00070

Moore PJ, Fenczik CA, Deom CM, Beachy RN. Developmental changes in plasmodesmata in transgenic tobacco expressing the movement protein of *Tobacco mosaic virus*. Protoplasma. 1992:**170**(3-4): 115–127. https://doi.org/10.1007/BF01378787

Movahed N, Cabanillas DG, Wan J, Vali H, Laliberté JF, Zheng H. Turnip mosaic virus components are released into the extracellular space by vesicles in infected leaves. Plant Physiol. 2019:**180**(3): 1375–1388. https://doi.org/10.1104/pp.19.00381

Niehl A, Amari K, Gereige D, Brandner K, Mély Y, Heinlein M. Control of *Tobacco mosaic virus* movement protein fate by CELL-DIVISION-CYCLE protein 48 (CDC48). Plant Physiol. 2012:**160**(4):2093–2108. https://doi.org/10.1104/pp.112.207399

Niehl A, Heinlein M. Perception of double-stranded RNA in plant antiviral immunity. Mole Plant Pathol. 2019:**20**(9):1203–1210. https://doi.org/10.1111/mpp.12798

Niehl A, Soininen M, Poranen MM, Heinlein M. Synthetic biology approach for plant protection using dsRNA. Plant Biotechnol J. 2018:**16**(9):1679–1687. https://doi.org/10.1111/pbi.12904

Niehl A, Wyrsch I, Boller T, Heinlein M. Double-stranded RNAs induce a pattern-triggered immune signaling pathway in plants. New Phytol. 2016:**211**(3):1008–1019. https://doi.org/10.1111/nph.13944

Nühse TS, Bottrill AR, Jones AM, Peck SC. Quantitative phosphoproteomic analysis of plasma membrane proteins reveals regulatory mechanisms of plant innate immune responses. Plant J. 2007:**51**(5): 931–940. https://doi.org/10.1111/j.1365-313X.2007.03192.x

Oparka KJ, Prior DAM, Santa Cruz S, Padgett HS, Beachy RN. Gating of epidermal plasmodesmata is restricted to the leading edge of expanding infection sites of *Tobacco mosaic virus*. Plant J. 1997:**12**(4), 781–789. https://doi.org/10.1046/j.1365-313X.1997.12040781.x

Pitzalis N, Heinlein M. The roles of membranes and associated cytoskeleton in plant virus replication and cell-to-cell movement. J Exp Bot. 2017:**69**(1):117–132. https://doi.org/10.1093/jxb/erx334

Rao S, Zhou Z, Miao P, Bi G, Hu M, Wu Y, Feng F, Zhang X, Zhou JM. Roles of receptor-like cytoplasmic kinase VII members in pattern-triggered immune signaling. Plant Physiol. 2018:**177**(4):1679–1690. https://doi.org/10.1104/pp.18.00486

Ruf A, Oberkofler L, Robatzek S, Weiberg A. Spotlight on plant RNA-containing extracellular vesicles. Curr Opin Plant Biol. 2022:**69**:102272. https://doi.org/10.1016/j.pbi.2022.102272

Sambade A, Brandner K, Hofmann C, Seemanpillai M, Mutterer J, Heinlein M. Transport of TMV movement protein particles associated with the targeting of RNA to plasmodesmata. Traffic. 2008:**9**(12): 2073–2088. https://doi.org/10.1111/j.1600-0854.2008.00824.x

Simpson C, Thomas C, Findlay K, Bayer E, Maule AJ. An Arabidopsis GPI-anchor plasmodesmal neck protein with callose binding activity and potential to regulate cell-to-cell trafficking. Plant Cell. 2009:**21**(2):581–594. https://doi.org/10.1105/tpc.108.060145

Tan X, Sun L, Chen J, Chen ZJ. Detection of microbial infections through innate immune sensing of nucleic acids. Annu Rev Microbiol. 2018:**72**(1): 447–478. https://doi.org/10.1146/annurev-micro-102215-095605

Thomas CL, Bayer EM, Ritzenthaler C, Fernandez-Calvino L, Maule AJ. Specific targeting of a plasmodesmal protein affecting cell-to-cell communication. PLoS Biol. 2008:**6**(1):e7. https://doi.org/10.1371/journal.pbio.0060007

Thor K, Jiang S, Michard E, George J, Scherzer S, Huang S, Dindas J, Derbyshire P, Leitao N, DeFalco TA, et al. The calcium-permeable channel OSCA1.3 regulates plant stomatal immunity. Nature. 2020:**585**(7826):569–573. https://doi.org/10.1038/s41586-020-2702-1

Tian W, Hou C, Ren Z, Wang C, Zhao F, Dahlbeck D, Hu S, Zhang L, Niu Q, Li L, et al. A calmodulin-gated calcium channel links pathogen patterns to plant immunity. Nature. 2019:**572**(7767):131–135. https://doi.org/10.1038/s41586-019-1413-y

Tilsner J, Nicolas W, Rosado A, Bayer EM. Staying tight: plasmodesmal membrane contact sites and the control of cell-to-cell connectivity in plants. Annu Rev Plant Biol. 2016:**67**(1):337–364. https://doi.org/10.1146/annurev-arplant-043015-111840

Tucker EB, Boss WF. Mastoparan induced intracellular ca^{2+} fluxes may regulate cell-to-cell communication in plants. Plant Physiol. 1996:**111**(2):459–467. https://doi.org/10.1104/pp.111.2.459

Uchiyama A, Shimada-Beltran H, Levy A, Zheng JY, Javia PA, Lazarowitz SG. The Arabidopsis synaptotagmin SYTA regulates the cell-to-cell movement of diverse plant viruses. Front Plant Sci. 2014:**5**:584. https://doi.org/10.3389/fpls.2014.00584

Vatén A, Dettmer J, Wu S, Stierhof YD, Miyashima S, Yadav SR, Roberts CJ, Campilho A, Bulone V, Lichtenberger R, et al. Callose biosynthesis regulates symplastic trafficking during root development. Dev Cell. 2011:**21**(6):1144–1155. https://doi.org/10.1016/j.devcel.2011.10.006

Vogler H, Akbergenov R, Shivaprasad PV, Dang V, Fasler M, Kwon MO, Zhanybekova S, Hohn T, Heinlein M. Modification of small RNAs associated with suppression of RNA silencing by tobamovirus replicase protein. J Virol. 2007:**81**(19):10379–10388. https://doi.org/10.1128/JVI.00727-07

Vogler H, Kwon MO, Dang V, Sambade A, Fasler M, Ashby J, Heinlein M. *Tobacco mosaic virus* movement protein enhances the spread of RNA silencing. PLoS Pathog. 2008:**4**(4):e1000038. https://doi.org/10.1371/journal.ppat.1000038

Wan J, Cabanillas DG, Zheng H, Laliberté J-F. Turnip mosaic virus moves systemically through both phloem and xylem as membrane-associated complexes. Plant Physiol. 2015:**167**(4): 1374–1388. https://doi.org/10.1104/pp.15.00097

Wan J, Laliberté J-F. Membrane-associated virus replication complexes locate to plant conducting tubes. Plant Signal Behav. 2015:**10**(8): e1042639. https://doi.org/10.1080/15592324.2015.1042639

Wang X, Sager R, Cui W, Zhang C, Lu H, Lee JY. Salicylic acid regulates plasmodesmata closure during innate immune responses in Arabidopsis. Plant Cell. 2013:**25**(6):2315–2329. https://doi.org/10.1105/tpc.113.110676

Wu SW, Kumar R, Iswanto ABB, Kim JY. Callose balancing at plasmodesmata. J Exp Bot. 2018:**69**(22):5325–5339. https://doi.org/10.1093/jxb/ery317

Xu B, Cheval C, Laohavisit A, Hocking B, Chiasson D, Olsson TSG, Shirasu K, Faulkner C, Gilliham M. A calmodulin-like protein

regulates plasmodesmal closure during bacterial immune responses. New Phytol. 2017:**215**(1):77–84. https://doi.org/10.1111/nph.14599

Yuan C, Lazarowitz SG, Citovsky V. The plasmodesmal localization signal of TMV MP is recognized by plant synaptotagmin SYTA. mBio. 2018:**9**(4):e01314-18. https://doi.org/10.1128/mBio.01314-18

Zhang J, Li W, Xiang T, Liu Z, Laluk K, Ding X, Zou Y, Gao M, Zhang X, Chen S, et al. Receptor-like cytoplasmic kinases integrate signaling from multiple plant immune receptors and are targeted by a *Pseudomonas syringae* effector. Cell Host Microbe. 2010:**7**(4): 290–301. https://doi.org/10.1016/j.chom.2010.03.007